

# Microstructural characteristics of belite–sulfoaluminate cement clinkers with bottom ash

Lea Žibret<sup>a,\*</sup>, Andrej Ipavec<sup>b</sup>, Sabina Dolenc<sup>a</sup>

<sup>a</sup> Slovenian National Building and Civil Engineering Institute, Dimičeva ulica 12, SI-1000 Ljubljana, Slovenia

<sup>b</sup> Salonit Anhovo d.d., Anhovo 1, SI-5210 Deskle, Slovenia

## ARTICLE INFO

### Keywords:

BCSA clinker  
Belite  
Calcium sulfoaluminate  
Secondary raw materials  
Microstructure  
Reactivity

## ABSTRACT

The incorporation mechanism of impurities derived from raw materials into a belite–sulfoaluminate cement clinker with bottom ash was investigated in two raw mixtures. Alkalis lowered the sintering temperature by 50 °C. Ti stabilized  $\beta$  belite and prevented the formation of  $\gamma$ -belite. Sodalite solid solution showed an incomplete substitution of Si by Al. At a higher Ti content ferrite solid solution trended towards perovskite composition. Although calcium sulfoaluminate only fully developed at 1300 °C, the clinkers sintered at 1200 °C were the most reactive, as the presence of anhydrite at 1200 °C accelerated early hydration. Clinker reactivity decreased with an increase in sintering temperature.

## 1. Introduction

Recently, many studies have focused on the development of low energy and low carbon binders with physical and mechanical properties comparable to those of ordinary Portland cement (OPC) e.g. belite–sulfoaluminate (BCSA) cements, which are also known as belite–ye’elimite–ferrite (BYF) cements [1–3]. Moreover, the raw BCSA clinker mixture allows for the incorporation of various secondary raw materials, therefore enabling the recycling of industrial waste [4–7].

The parameters that influence the reactivity of a BCSA clinker can generally be divided into two groups: (i) phase composition, i.e. the ratio between belite and calcium sulfoaluminate, and (ii) clinker microstructure, i.e. the grain size and morphology of phases, phase distribution, and the incorporation of foreign ions into the clinker phases [8]. The belite ( $C_2S$ ) phase represents > 50 wt% of the BCSA clinker [2]. Without doping, belite is presented in its  $\beta$  modification, which might be partly transformed into the  $\gamma$  modification during the cooling process [9]. If there is a sulphate surplus in the raw clinker mixture, however, some of the belite can be replaced by ternesite [10], which is also a reactive clinker phase [11]. The second most abundant phase of the BCSA clinker is calcium sulfoaluminate ( $C_4A_3\dot{S}$ ) [2], which appears in both cubic and orthorhombic form [12,13]. Calcium sulfoaluminate is an artificial analogue of the mineral Ye’elimite, an end member of

sodalite ( $Na_8(Al_6Si_6O_{24})Cl_2$ ) in which  $Na^+$  and  $Si^{4+}$  are replaced by  $Ca^{2+}$  and  $Al^{3+}$ , respectively [14,15]. Another hydraulic phase of the BCSA clinker is ferrite ( $C_4AF$ ) [2]. Periclase (M), gehlenite ( $C_2AS$ ), mayenite ( $C_{12}A_7$ ), perovskite (CT), arcanite (K $\dot{S}$ ), acermanite, magnetite and anhydrite (C $\dot{S}$ ) are the minor phases most commonly reported [12,16]. During the thermal decomposition of the sulfur-bearing phases the loss of  $SO_3$  can influence the thermodynamic balance and formation of the clinker phases [17,18].

In general, the microstructure of the BCSA clinker is formed by the reaction from solid–solid to liquid–solid state [8]. Belite usually forms irregularly shaped crystals with clear margins, calcium sulfoaluminate forms angular hexagonal crystals, while ferrite sometimes forms large bright crystals with irregular shapes and clear margins [5,8,19–21]. More commonly, ferrite is present as an interstitial phase, indicating the presence of liquid at the clinkering temperature chosen [22]. With regard to the minor phases, dark periclase grains are occasionally evident on the SEM/BSE images [8].

BCSA clinker, prepared from impure raw materials such as secondary raw materials, commonly incorporates foreign elements in the main clinker phases which can modify the temperature of the ferrite formation and/or the amount of melt, change the rate of the reactions occurring in the solid state within the liquid–solid interface, and alter the viscosity and surface tension of the melt, consequently affecting the

*Abbreviations:* OPC, Ordinary Portland cement; CSA, Calcium sulfoaluminate; BCSA, Belite–sulfoaluminate; BYF, Belite–ye’elimite; SEM, Scanning electron microscopy; BSE, Back-scattered electron detector; EDS, Energy-dispersive X-ray spectroscopy; LOI, Loss on ignition; PSD, Particle size distribution.

\* Corresponding author..

E-mail addresses: [zibret.lea@gmail.com](mailto:zibret.lea@gmail.com) (L. Žibret), [andrej.ipavec@salonit.si](mailto:andrej.ipavec@salonit.si) (A. Ipavec), [sabina.dolenc@zag.si](mailto:sabina.dolenc@zag.si) (S. Dolenc).

<https://doi.org/10.1016/j.conbuildmat.2021.126289>

Received 18 December 2020; Received in revised form 9 November 2021; Accepted 29 December 2021

Available online 14 January 2022

0950-0618/© 2022 The Author(s). Published by Elsevier Ltd. This is an open access article under the CC BY license (<http://creativecommons.org/licenses/by/4.0/>).

growth and morphology of the crystals [23–25]. Foreign ions incorporated into clinker phases from impurities in the material can also influence the hydraulic properties of the material [4,5,26–29]. Belite can incorporate S, Al, Fe, Ti, P, Mg and alkali into the crystal structure [8,30,31], calcium sulfoaluminate commonly incorporates Fe, Na, and Si [8,32–35], while Ti, Mg and Mn can be found in ferrite [8]. It has been reported that foreign iron ions strongly impact the reactivity of the calcium sulfoaluminate phase [16,33].

The existing studies regarding BCSA clinkers investigate the individual parameters that influence the clinker microstructure. Some studies have therefore focused on phase composition and its influence on the reactivity of the clinker and/or cement [11,12,27,36]. The grain size distribution of belite, calcium sulfoaluminate and ferrite, and the incorporation of foreign ions into calcium sulfoaluminate (CSA) clinkers has mostly been described in a range of studies on the formation of solid solutions inside the equilibrium phase assemblage of lime-belite-calcium sulfoaluminate-ferrite-anhydrite [8]. The incorporation of various foreign ions, including Al, B, P, Fe, S or/and K [28], into CSA clinkers has been studied across a range of doping levels [4,12]. The impurities also exert a strong influence on which of the numerous polymorphs are obtained – the effects of chemical-stabilising ions on the stability of  $\beta$ -phase belite have been investigated extensively [37,38]. Several theoretical predictions have been made regarding which ions can stabilize  $\beta$ -belite, suggesting  $B_2O_3$ ,  $Na_2O$ ,  $K_2O$ ,  $BaO$ ,  $MnO_2$  and  $Cr_2O_3$ , or combinations thereof [38]. The influence of incorporating Ti in the belite phase of BCSA clinkers, however, has not yet been satisfactorily studied. There is no systematic or detailed study investigating the microstructure of BCSA clinkers available in the literature [21]. In the studies mentioned above the clinkers were mostly prepared from reagent grade materials, while very few studies have been conducted where the BCSA clinker is made from natural and secondary raw materials.

Huge amounts of coal ash (fly ash and bottom ash) are generated globally through coal combustion processes in thermal power-plants. Moreover, its rate of production is still increasing. Because of its low cost, availability and property-enhancing characteristics, fly ash is commonly used in the construction sector as a substitute for clinker. The low reactivity of bottom ash, however, makes it less usable for this purpose, and it is therefore more commonly used for the partial replacement of fine aggregates in concrete [39]. Additionally, coal bottom ash is not used as a constituent of cement because it is not covered by particular standards. Large quantities of bottom ash are therefore not used in any form and are still stored in the ash dumps [40], causing serious environmental problems including air, water and soil pollution [41]. In 2016 over 3500 kilotonnes of bottom ash was generated from coal combustion processes in Europe alone [42]. The physical, chemical and mineral properties of coal bottom ash can vary between different power plants as they use different types and sources of coal and apply different burner operating conditions [43].

Since BCSA clinkers from class C fly ash (>20% CaO) have been shown to be far more reactive than clinkers prepared from reagent grades [36], the incorporation of bottom ash into the BCSA clinker raw mix seems to be a promising solution for the reuse of bottom ash. There are, however, only a few studies evaluating the incorporation of coal combustion residuals into BCSA clinkers, which investigate the incorporation of fly ash into clinker raw mixtures [11,27,44–46]. Although a lot of bottom ash is available from dumps worldwide, and it is suitable for use in various construction composites [47], studies focussing on the use of bottom ash in BCSA clinkers are not yet available. A few existing studies that used bottom ash as the starting material to synthesize belite and calcium sulfoaluminate were based on other processes, for example hydrothermal calcination [48].

This paper investigates the microstructure and phase development of BCSA clinkers synthesised at three different temperatures, analysed by X-ray powder diffraction (Rietveld refinement) and scanning electron microscopy. The incorporation of minor elements was studied by energy

dispersive X-ray spectroscopy (EDS). Furthermore, the hydraulic activity of the clinker without added sulfate was investigated by isothermal calorimetry. Hydration curves of the two clinker compositions at the three sintering temperatures were compared at a similar fineness in order to evaluate the influence of phase composition and microstructural variations, as well as the incorporation of minor ions, on clinker reactivity.

## 2. Experimental

### 2.1. Raw materials

The main raw materials used in this study were limestone and flysch (alternating layers of calcareous breccia, calcareous sandstones and marls [49]), coal combustion bottom ash, and white titanogypsum. Bauxite and mill scale were used for the correction of the aluminium and iron in the raw meal (Table 1). In order to prepare a batch of homogeneous raw materials, 5 kg of each material was milled in a ball mill, following the criteria that 95 wt% of the material could pass through a 200  $\mu$ m sieve. The chemical compositions of the raw materials used are given in Table 1.

### 2.2. Synthesis of the clinkers

The targeted phase composition of the KBA1 and KBA2 clinkers prepared are given in Table 2. The raw mixtures (calculated to Total = 95 wt%) were formulated according to a generalized Bogue calculation for sulfoaluminate cements based on fly ash [50] and are given in Table 1. 200 g of each mixture was homogenized in a laboratory ball mill (steel balls; CAPCO Test Equipment Ball Mill Model 9VS) for 3 h, using 200 ml isopropanol as the grinding media. The isopropanol was removed by vacuum drying (using 1 medium permeable laboratory paper) followed by oven drying overnight at 40 °C. Pressed pellets were prepared using a HPM 25/5 press at 15 MPa. 15 g of material was used for each pellet. The clinker mixtures were subjected to heating up to 1200 °C, 1250 °C, and 1300 °C in a Protherm furnace PLF 160/9 at a heating rate of 10 °C/min, held at the final temperature for 60 min, and then cooled in the closed furnace.

### 2.3. Methods

The phase composition of the clinker samples synthesized was determined by a PANalytical Empyrean X-ray diffractometer equipped with  $CuK\alpha$  radiation with a wavelength of  $\lambda = 1.54 \text{ \AA}$ . Around 10 g of the samples were ground in an agate mortar to a particle size below 0.063 mm. The ground powder was manually back-loaded into a circular sample holder (diameter of 16 mm) in order to mitigate the preferred orientation effect for X-ray diffraction data collection. The optical configuration consisted of a large soller slit (0.04 rad), a fixed divergence slit ( $1/2^\circ$ ), a fixed incident anti scatter slit ( $1^\circ$ ), and a PIXcel1D-Medipix3 detector working in scanning mode with an active length of  $3.3473^\circ \times 2\theta$  and a large soller slit (0.04 rad). Data for each sample were collected from  $4^\circ$  to  $70^\circ$  ( $2\theta$ ). During data collection the samples were rotated using a revolution time of 2 s in order to enhance the particle statistics. The X-ray tube worked at 45 kV and 40 mA. Rietveld refinements were performed using PANalytical X'Pert High Score Plus diffraction software v. 4.8, using the structures for the phases from ICDD PDF 4 + 2016 RDB powder diffraction files. The powder diffraction file (PDF) codes used for Rietveld refinements for the identified phases were:  $\beta$ - $C_2S$  (04-007-2687),  $\gamma$ - $C_2S$  (04-010-9508),  $C_4A_3S$ -orthorhombic (04-011-1786),  $C_4A_3S$ -cubic (04-009-7268),  $C_4AF$  (04-006-8923), M (01-071-1176), CT (04-007-5451),  $C_{12}A_7$  (01-070-2144), K $\acute{S}$  (04-006-8317), KN $\acute{S}$  (04-007-4249),  $C_2AS$  (01-077-1147), C $\acute{S}$  (01-072-0916), and C (00-037-1497). The amorphous phase was not considered.

SEM/EDS analysis was performed in order to study the morphology,

**Table 1**

Composition of the raw materials with respect to the primary oxides, loss on ignition (LOI) at 950°, and the proportions of raw materials in mixtures KBA1 and KBA2 (wt%).

Raw material	CaO	SiO <sub>2</sub>	Al <sub>2</sub> O <sub>3</sub>	Fe <sub>2</sub> O <sub>3</sub>	SO <sub>3</sub>	MgO	K <sub>2</sub> O	Na <sub>2</sub> O	TiO <sub>2</sub>	MnO	LOI	KBA1	KBA2
Limestone	51.51	4.76	0.86	0.51	0.09	0.90	0.14	0.81	0.04	0.04	41.41	57.9	59.1
Flysch	28.83	32.02	7.74	3.49	0.07	1.69	1.33	0.54	0.38	0.07	24.65	23.6	11.5
Bottom ash	5.63	59.75	18.73	10.03	0.15	2.20	1.70	1.01	0.73	0.10	1.20	9.0	9.2
White titanogypsum	32.62	0.13	1.16	0.04	45.39	0.04	0.01	0.26	0.72	0.01	21.35	4.0	7.0
Bauxite	0.06	5.88	87.69	1.89	0.17	0.52	0.39	0.08	3.81	0.01	0.15	5.3	12.6
Mill scale	0.82	0.64	0.34	97.96	0.09	0.00	0.01	0.00	/	b.d.l.	0.00	0.2	0.6

**Table 2**

Clinker phase composition determined by Rietveld method and targeted phase compositions of the raw mixtures (wt%). Clinker phase designations:  $\beta$ -C<sub>2</sub>S =  $\beta$ -belite;  $\gamma$ -C<sub>2</sub>S =  $\gamma$ -belite; C<sub>2</sub>S = belite; C<sub>4</sub>A<sub>3</sub>S<sup>cub.</sup> = cubic calcium sulfoaluminate; C<sub>4</sub>A<sub>3</sub>S<sup>or.</sup> = orthorhombic calcium sulfoaluminate; C<sub>4</sub>A<sub>3</sub>S<sup>cub.</sup> = calcium sulfoaluminate; C<sub>4</sub>AF = ferrite; M = periclase; C<sub>12</sub>A<sub>7</sub> = mayenite; CT = perovskite; K<sup>S</sup> = arcanite; K<sup>NS</sup> = aphthitalite; C<sub>2</sub>AS = gehlenite; C<sup>S</sup> = anhydrite; C = free lime.

Raw mixture	Method	Sintering T (°C)	$\beta$ -C <sub>2</sub> S	$\gamma$ -C <sub>2</sub> S	$\Sigma$ C <sub>2</sub> S	C <sub>4</sub> A <sub>3</sub> S <sup>cub.</sup>	C <sub>4</sub> A <sub>3</sub> S <sup>or.</sup>	$\Sigma$ C <sub>4</sub> A <sub>3</sub> S	C <sub>4</sub> AF	M	C <sub>12</sub> A <sub>7</sub>	CT	K <sup>S</sup>	K <sup>NS</sup>	C <sub>2</sub> AS	C <sup>S</sup>	C
KBA1	Rietveld	1200	65.7	0.1	65.8	7.8	10.6	18.4	9.6	1.3	0.9	0.5	1.1	0.7	0.6	1.2	0.0
		1250	64.2	1.4	65.5	10.6	9.5	20.0	10.2	1.4	/	0.1	1.1	0.3	0.7	0.7	0.0
		1300	64.9	1.6	66.5	7.9	9.7	17.5	9.6	1.4	0.7	0.4	1.6	0.9	0.8	0.5	0.0
KBA2	Rietveld	1200	56.3	0.0	56.3	10.9	19.8	30.7	4.1	1.4	3.5	1.8	1.3	0.5	0.4	0.0	0.1
		1250	51.7	0.0	51.7	16.2	19.4	35.6	8.0	1.3	0.7	1.1	1.3	0.3	0.1	0.0	0.1
		1300	48.6	0.6	49.2	13.6	21.4	34.9	10.8	1.2	2.0	0.5	1.1	0.3	0.0	0.1	0.1
KBA1	Targeted compos.				65		20	10									
KBA2	Targeted compos.				50		35	10									

size and distribution of the phases, as well as the incorporation of minor elements in the clinker phases. Uncoated polished cross-sections of the clinker pellets in vertical profiles were examined by a JEOL IT500 LV Scanning Electron Microscope (SEM) equipped with an Energy Dispersive X-ray spectrometer (EDS) with a W-filament, operated in low vacuum mode at an accelerating voltage of 20 kV and a working distance of 10 mm. Grain diameter was measured using the AZtec software "ruler" tool and grain size distribution was further processed using Excel software. The general elemental distribution of clinkers was determined by EDS elemental mapping, while data for the detailed EDS elemental composition of the main clinker phases were collected by EDS point analysis of a large number of belite, calcium sulfoaluminate and ferrite grains, measured on various parts of the clinker.

The reactivity of the synthesized clinkers was assessed by isothermal conduction calorimetry using an eight-channel TAM Air 8 calorimeter (TA Instruments). Samples were ground in a laboratory disc mill (Siebtechnik) using a uniform procedure; 50 g of crushed clinker was ground for 6 s and sieved to < 125  $\mu$ m, then the residue was ground again for another 6 s until all the sample passed through a 125  $\mu$ m sieve. 8 g of the ground clinker and 4 g of distilled water (w/c 0.5) were then hand mixed for 5 min and 6 g of the mixture was placed into the calorimeter. The heat evolution was evaluated for 7 days at 20 °C. Due to the external mixing approach the early heat of hydration, i.e. up to 30 min, was not observed. The particle size distribution (PSD) of the ground clinkers was measured by laser diffraction granulometry using a HELOS/BR + RODOS/M + VIBRI SYMPATEC laser grain-size analyser with a size range from 0.1 to 875  $\mu$ m. Analyses of bulk samples (around 10 g) were performed in the dry dispersion measurement mode. The fineness of the ground clinkers, expressed in terms of the specific surface area, was determined using the Blaine air-permeability apparatus ToniPERM Standard Model 6578.

### 3. Results and discussion

#### 3.1. X-ray powder diffraction

The results of the X-ray powder diffraction analysis are given in Table 2. Additionally, an example XRD pattern for clinker KBA1 sintered

at 1300 °C is shown on Fig. 1. XRD patterns of KBA1 at the other temperatures and of KBA2 at all temperatures are omitted so as to avoid data duplication. Belite predominantly appeared in  $\beta$ -form ( $\beta$ -C<sub>2</sub>S) in both mixtures at all three sintering temperatures (1200 °C, 1250 °C and 1300 °C). However,  $\gamma$ -belite ( $\gamma$ -C<sub>2</sub>S) was also detected in minor amounts. Calcium sulfoaluminate (C<sub>4</sub>A<sub>3</sub>S) was present in cubic and orthorhombic polymorphs. Of the minor phases periclase (M), arcanite (K<sup>S</sup>), mayenite (C<sub>12</sub>A<sub>7</sub>), perovskite (CT), anhydrite (C<sup>S</sup>), aphthitalite (K<sup>NS</sup>), gehlenite (C<sub>2</sub>AS) and free lime (C) were detected in different proportions.

In the KBA1 mixture the targeted amounts of belite, calcium sulfoaluminate and ferrite were already formed at 1200 °C and their content did not significantly change by increasing the sintering temperature, while in the clinkers made from the KBA2 mixture the amount of major phases varied as the temperature increased. Belite can form five temperature dependent polymorphs under ambient conditions [51]. The  $\alpha'$  modification has been shown to form at the sintering temperatures of the BCSA clinkers, but is transformed into  $\beta$  modification with cooling below 850 °C [9]. Belite has been shown to form in the BCSA clinker in the temperature range of 1000–1200 °C and calcium sulfoaluminate between 1000 and 1250 °C [52]. Calcium sulfoaluminate is cubic at room temperature [13]. The orthorhombic calcium sulfoaluminate content remained constant with the increase in temperature in both clinker mixtures, while in both cases the highest amount of cubic calcium sulfoaluminate was detected at 1250 °C. As ionic exchanges can restore the cubic symmetry in calcium sulfoaluminate [53], this could indicate that the maximum incorporation rate of minor elements took place at 1250 °C in both clinkers. It has been reported that pseudo-cubic calcium sulfoaluminate reacts at a higher rate than the orthorhombic form [54–56]. In KBA1 the targeted amount of belite was reached at 1200 °C, and this did not change by increasing the temperature. In KBA2, on the other hand, the belite content decreased with an increase in temperature, approaching the targeted amount at 1250 °C. Similar to belite, the targeted amount of calcium sulfoaluminate was reached in KBA1 at 1200 °C and did not change by increasing the temperature, while in KBA2 the calcium sulfoaluminate content increased as the temperature increased, achieving the final amount at 1250 °C. Moreover, as for both belite and calcium sulfoaluminate, in

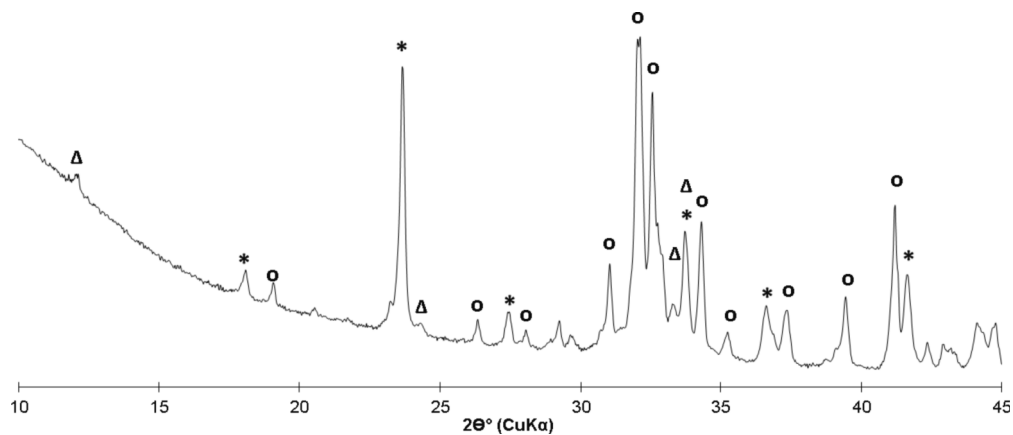


Fig. 1. XRD pattern for clinker KBA1 sintered at 1300 °C. Main clinker phase designations: o = belite; \* = calcium sulfoaluminate; Δ = ferrite.

KBA1 the targeted amount of ferrite was reached at 1200 °C and did not change with an increase in temperature, while in the KBA2 clinker the amount of ferrite increased by increasing the sintering temperature and its targeted amount was reached only at 1250–1300 °C. The elevated alkali content in the KBA1 mixture, originating from the higher proportion of flysch, could however be responsible for the formation of ferrite at a lower temperature compared to that of KBA2 [23,24]. The different behaviour of the ferrite phase in the clinkers could be partly attributed to the influence of the phase composition, namely the higher content of calcium sulfoaluminate in the KBA2 and consequently the different crystallization paths, which result from the coexistence of calcium sulfoaluminate and ferrite solid solutions [57,58]. The elevated Ti content in the KBA2 mixture, on the other hand, can promote trending of the ferrite solid solution towards the formation of perovskite [59–62], and consequently lower the amount of ferrite in this mixture (Table 2).

With regard to the minor phases, periclase was generally constant in both mixtures at all sintering temperatures, while gehlenite was detected predominately in the KBA1 mixture, with its maximum content at 1300 °C. In contrast to KBA1, gehlenite was not detected in KBA2 at a sintering temperature of 1300 °C, while at lower temperatures it was observed in quantities similar to in KBA1. Gehlenite forms in BCSA clinkers together with belite in the temperature interval 800–900 °C, while above 1000 °C it disappears [52]. At all three sintering temperatures gehlenite was therefore not stable and probably formed during the clinker cooling process [63]. Mayenite appeared as an intermediate phase in both KBA1 and KBA2. In both types of clinker the maximum amount of mayenite was detected at 1200 °C, while at 1250 °C it was barely perceptible. At 1300 °C the amount of mayenite increased. Mayenite forms at 1000–1100 °C through the reaction of calcium aluminate and free lime [52]. It decreases along with an increasing temperature and disappears at 1250 °C [64], when it reacts with anhydrite to form the calcium sulfoaluminate phase [52]. In the calcium sulfoaluminate-rich clinkers, however, mayenite was detected even above 1250 °C [65], which could be attributed to the decomposition of the calcium sulfoaluminate phase at around 1250 °C [52]. The amount of mayenite in KBA2 was significantly higher than in KBA1, which could be attributed to the higher cubic calcium sulfoaluminate content in the KBA2 mixture [56]. The XRD results for KBA2 revealed an increase in mayenite and simultaneously a decrease in calcium sulfoaluminate at the temperature interval between 1250 and 1300 °C (Table 2). At the same time, some anhydrite was detected in KBA2 at 1300 °C (Table 2), which could be explained by the onset of calcium sulfoaluminate decomposition at 1250 °C in this sample. Consequently, mayenite and anhydrite were formed (Table 2). The very small quantity of anhydrite detected in KBA2 (Table 2), however, could also be attributed to the volatilisation of sulfur oxide between 1200 and 1300 °C, which can be accelerated by the increased Fe<sub>2</sub>O<sub>3</sub> content in the raw mixture [58]. On

the other hand, mayenite and anhydrite were barely perceptible at 1300 °C in KBA1 (Table 2), which can be attributed to the lower proportion of calcium sulfoaluminate in the raw mixture. The small quantity of free lime presented in KBA2 could indicate the partial decomposition of mayenite into calcium aluminate, accompanied by free lime, during clinker cooling [52]. The amount of calcium aluminate was, however, probably very small and thus could not be detected by X-ray powder diffraction analysis (Table 2).

Perovskite was generally constant across all temperatures in KBA1, while in KBA2 its content decreased in line with an increase in temperature, in direct contrast to ferrite, which increased by increasing the temperature in KBA2. With respect to the minor phases, some alkali sulphates (arcanite, apthitalite) were detected in both clinker mixtures. Anhydrite was found only in KBA1, where its amount decreased by increasing the sintering temperature, as it was consumed during the crystallization of the calcium sulfoaluminate phase. A small quantity of free lime was detected in KBA2 at all sintering temperatures, while it was not present in KBA1 (Table 2).

The results revealed that all the main clinker phases were already fully developed at 1200 °C in the KBA1 mixture, whereas this only occurred at 1250 °C in the KBA2 mixture (Table 2). The reason for the lower optimal sintering temperature of the KBA1 clinkers, by approximately 50 °C, could be the higher alkali content of the KBA1 raw mixture, introduced mainly by flysch (Table 1), since alkalis can modify the physicochemical properties of the melt and affect the phase composition of the clinker [66].

The formation of the clinker's minor phases strongly depends on the impurities of the raw material. The formation of periclase, for instance, can mainly be attributed to Mg derived from bottom ash and flysch (Table 1). The proportion of bottom ash is, however, similar in the KBA1 and KBA2 mixtures, as the amount of periclase in KBA1 and KBA2 is similar. The formation of perovskite can be correlated to the Ti derived from bauxite (Table 1), which is more common in KBA2 due to the higher proportion of bauxite used in this mixture (Table 1). Moreover,  $\gamma$ -belite was far more common in KBA1, while in KBA2 a small amount of  $\gamma$ -belite was presented only at 1300 °C (Table 2). The absence of  $\gamma$ -belite in KBA2 can be explained by the elevated content of impurities, such as Ti, which can stabilize  $\beta$ -belite [44]. Despite the fact that Na<sub>2</sub>O and K<sub>2</sub>O can also stabilize  $\beta$ -belite [38], in our case it is unlikely, because although the alkali content is higher in KBA1 compared to KBA2 (Table 1),  $\beta$ -belite is more stable in the latter.

### 3.2. SEM/EDS

#### 3.2.1. The influence of sintering temperature on clinker microstructure

All clinker samples showed a fine-grained (aphanitic) texture. At a sintering temperature of 1200 °C KBA1 had an open pore structure,

while at 1250 °C the pores were irregularly-shaped, commonly elongated, and up to 50 µm in diameter (Fig. 3b). In KBA2 the pores were open at 1200 °C and 1250 °C (Fig. 2a). At a sintering temperature of 1300 °C clinkers from both mixtures developed predominately circular and ellipse shaped pores up to 30 µm long, and smaller irregularly shaped pores up to 10 µm long, which appeared between the clinker phases. A clear decrease in porosity and an increase in clinker density was evident with the increasing sintering temperature in both mixtures.

KBA2 was, however, more porous than KBA1 at all sintering temperatures (Fig. 2). Densification of the microstructure led to a drop in connectivity between the pore spaces, which resulted in a reduction in the number of open pores [67]. While in KBA1 the microstructure continuously densified with the increasing temperature, a smaller change was observed in the microstructure of the KBA2 sample between 1200 and 1250 °C, in accordance with the results of X-ray powder diffraction analysis, which showed that the targeted phase composition was

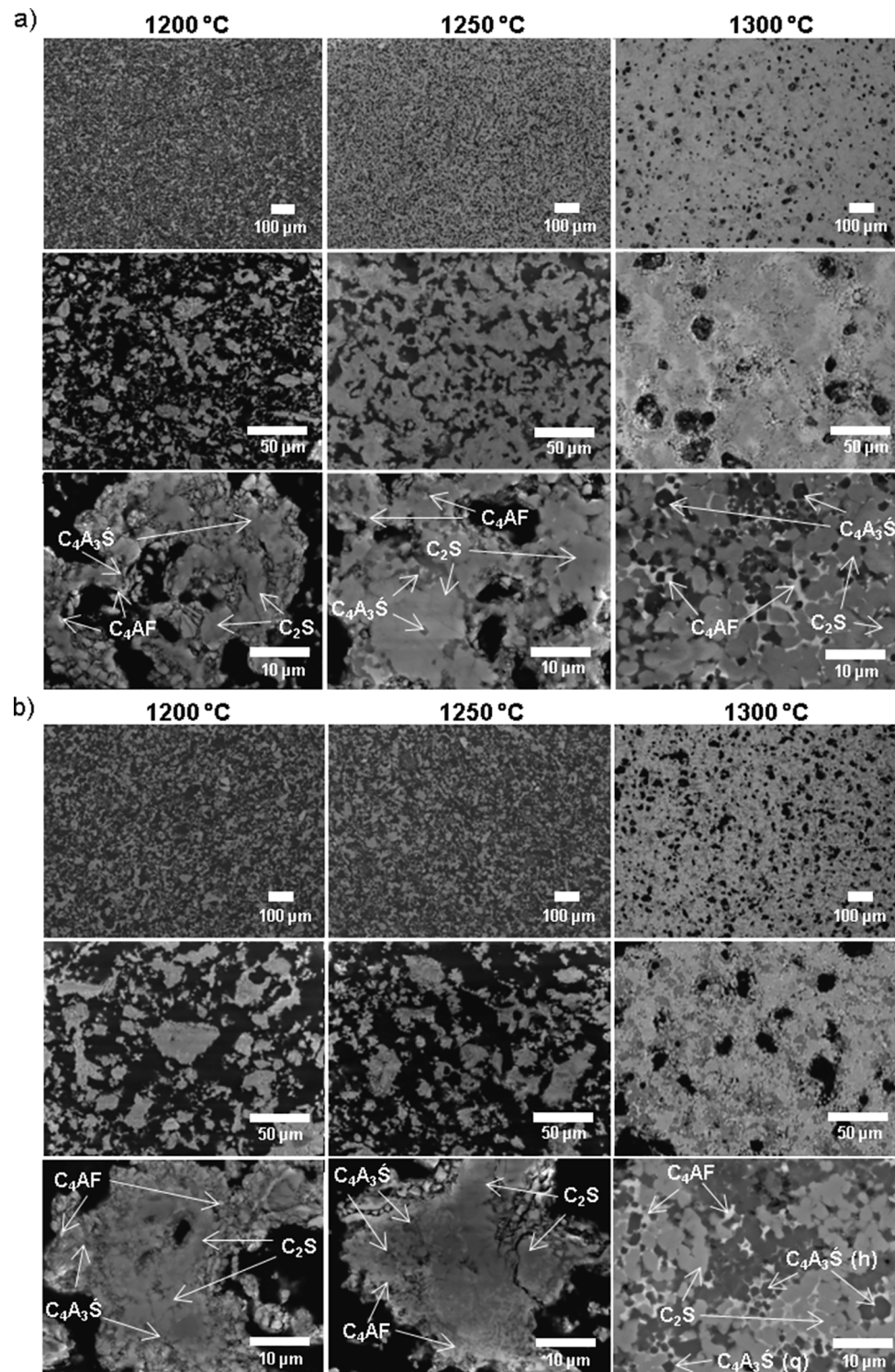


**Fig. 2.** KBA1 (a) and KBA2 (b) sintered at 1200, 1250 and 1300 °C at different magnifications. Clinker phase designations:  $C_2S$  = belite;  $C_4A_3S$  = calcium sulfoaluminate;  $C_4A_3S$  (h) = calcium sulfoaluminate (hexagonal cross-sections);  $C_4A_3S$  (q) = calcium sulfoaluminate (quadrangular cross-sections);  $C_4AF$  = ferrite.

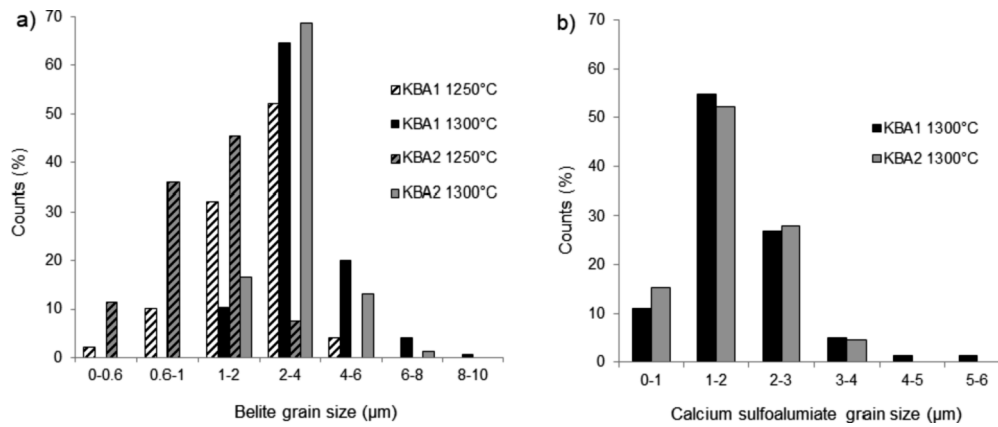


Fig. 3. Grain size distribution of belite at sintering temperatures of 1250 °C and 1300 °C (a) and of the calcium sulfoaluminate phase at 1300 °C (b).

reached at a higher temperature in this clinker composition. Additionally, the reduction in porosity could contribute to the formation of the liquid phase, which is suggested to form at a lower temperature due to the greater introduction of alkalis in the KBA1 raw mixture. As evidenced from the X-ray powder diffraction results, in KBA2 the amount of ferrite increased with an increase in sintering temperature.

As seen from Fig. 2, the belite grains differed according to the sintering temperature. Moreover, the increase in belite grain size was evident for both clinker compositions (Fig. 3a). At 1200 °C the prevailing belite grains had unclear boundaries, changing to anhedral to subhedral at 1250 °C and subhedral to euhedral at 1300 °C. At 1250 °C most of the belite grains had a diameter of 2–4 μm in KBA1, compared to the smaller grains of KBA2, most of which had a diameter of 1–2 μm (Fig. 3a), evidencing the higher development of the KBA1 microstructure at this temperature. At 1300 °C most of the belite grains were 2–4 μm in diameter, the same as in KBA1 at 1250 °C, in both clinker compositions (Fig. 3a). The change in grain size from 1250 to 1300 °C was significantly higher in the KBA2 mixture, suggesting a slower sintering reaction compared to KBA1. The subhedral belite grains were mostly rounded at 1250 °C, while some grains also presented as subangular and subrounded. Euhedral belite grains showed quadrangular and hexagonal cross-sections. At sintering temperatures of 1200 °C and 1250 °C calcium sulfoaluminate formed as an interstitial phase between the grains of belite. At 1300 °C subhedral to euhedral grains with quadrangular and hexagonal cross-sections or anhedral crystals developed between the belite, most of which measured 1–2 μm in diameter in both KBA1 and KBA2 (Fig. 2, Fig. 3b). Ferrite commonly formed an anhedral interstitial phase between the belite and calcium sulfoaluminate at all sintering temperatures (Fig. 2).

In accordance with the targeted and actual phase compositions, as determined by the Rietveld method (Table 2), the amount of belite was higher in KBA1, while the amount of calcium sulfoaluminate was higher in KBA2, which was especially evident at sintering temperatures of 1250 and 1300 °C (Fig. 2, Table 2). Some fractured belite grains, attributed to its gamma modification, were also found in KBA1. Ferrite was clearly evident in KBA1 at all sintering temperatures (Fig. 2a), which was supported by the constant amount of ferrite detected by the Rietveld method (Table 2). On the other hand, ferrite was barely visible in KBA2 at 1200 °C (Fig. 2b), with only 4 wt% determined by Rietveld refinement (Table 2). The amount of ferrite in KBA2 increased with a rising sintering temperature (Fig. 2, Table 2). In contrast to ferrite, perovskite was more abundant at a low temperature (Fig. 2, Table 2). At 1200 and 1250 °C other minor phases were too small for a reliable estimate of their incidence using SEM/EDS.

### 3.2.2. Microstructure at a sintering temperature of 1300 °C

The microstructures of KBA1 and KBA2 differed at 1300 °C, since the belite/calcium sulfoaluminate ratio varied as a result of the difference in

targeted phase compositions (Table 2).

The microstructure of the KBA1 clinker was homogeneous (Fig. 4a, b). The main constituent was belite (Fig. 4c), evident by the presence of subhedral to euhedral rounded grains 1–10 μm in length, with the highest proportion in the range of 2–4 μm (Fig. 3a). In places the belite grains were connected by their necks [68] (Fig. 4d). In some places smaller belite grains were surrounded by the calcium sulfoaluminate phase, indicating that the enclosing sulfoaluminate phase was younger (Fig. 4d, e).

Calcium sulfoaluminate (Fig. 4c) formed grains of up to 6 μm in length, predominately euhedral and less commonly subhedral, with the highest proportion sized between 1 and 2 μm (Fig. 3b). In KBA1 calcium sulfoaluminate crystals most commonly appeared as individual grains, while less commonly it contacted adjacent grains by “neck boundaries” or formed anhedral crystals filling the interstitial areas between other grains, usually belite (Fig. 4e). In some parts calcium sulfoaluminate grew over small belite grains (Fig. 4d, e).

Ferrite (Fig. 4c) appeared as the interstitial phase, which xenomorphically filled the area between the belite and calcium sulfoaluminate phases (Fig. 4c, e, f).

With respect to the minor phases, individual, unevenly distributed subhedral grains of periclase 2–5 μm in length appeared between the grains of belite and calcium sulfoaluminate (Fig. 4g). Moreover, needle-like fibrous gehlenite crystals, approximately 1–3 μm in length, formed in the interstitial area between the grains of calcium sulfoaluminate and belite. The fact that gehlenite grew over the grains of belite and calcium sulfoaluminate, and its rather preferred orientation, indicate the late-stage formation of gehlenite from a melt, probably during clinker cooling (Fig. 4h). Namely, since gehlenite is not stable at  $T > 1200$  °C [39], its formation was attributed to the decomposition of the calcium sulfoaluminate phase. In some parts of the clinker, the dark interstitial phase mayenite appeared between the calcium sulfoaluminate grains (Fig. 4i).

The microstructure of KBA2 was less homogeneous than the microstructure of KBA1 (Fig. 5a, b). As the most abundant phase, belite (Fig. 5c) had subhedral to euhedral predominately rounded and sub-rounded grains, 1–8 μm in length, with the highest proportion in the range 2–4 μm (Fig. 3a). In some places belite grains contacted in “neck boundaries”, similar to in KBA1 (Fig. 5d). In many parts, however, belite grains formed elongated contacts with wider “neck boundaries”, as observed in KBA1. Small belite grains were commonly surrounded by the calcium sulfoaluminate phase (Fig. 5e, i).

Calcium sulfoaluminate (Fig. 5c) formed predominately euhedral isometric or hexagonal grains up to 4 μm in length, with the highest proportion in the 1–2 μm range (Fig. 3b). Calcium sulfoaluminate grains were commonly concentrated in groups, with individual crystals being rare. It often developed “neck boundaries” with neighbouring grains or anhedral crystals filled the interstitial areas (Fig. 5e). In some parts it

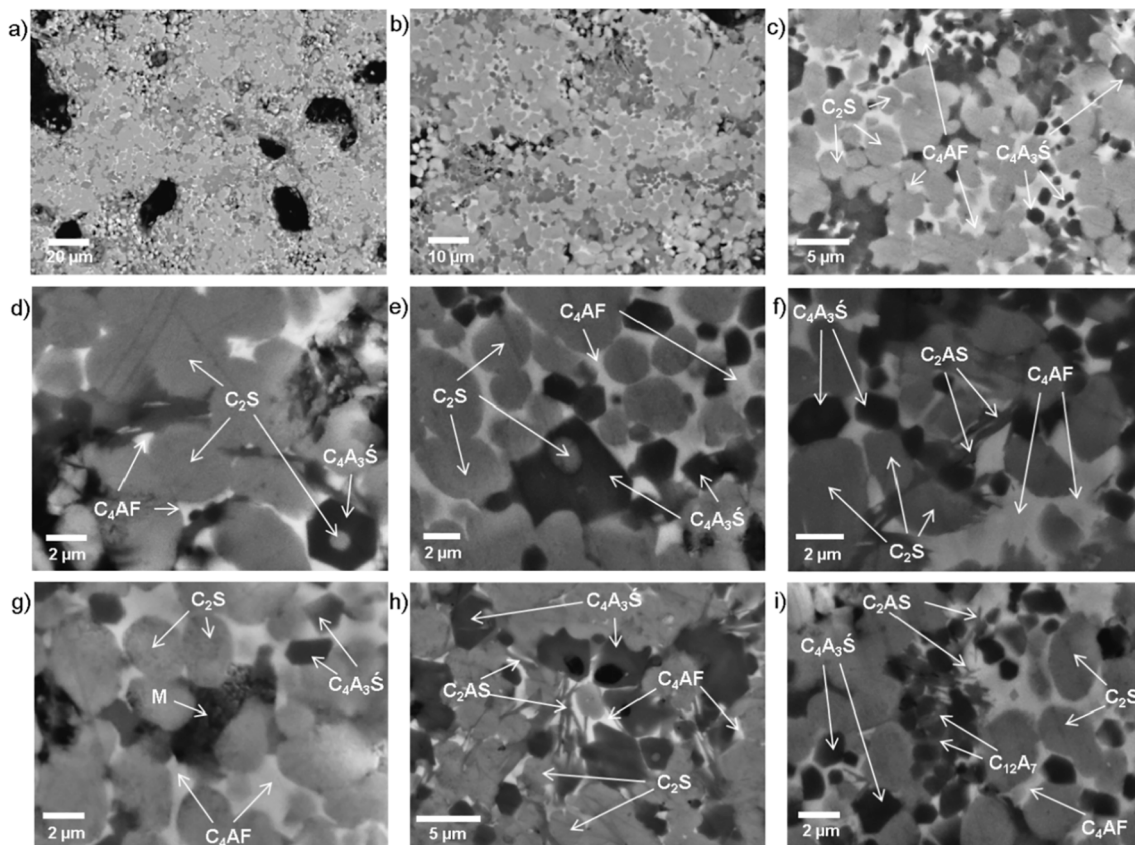


**Fig. 4.** General microstructure (a–c) and microstructural details of KBA1 sintered at 1300 °C: d) Belite ( $C_2S$ ) grains with “neck boundaries” and belite enclosed in calcium sulfoaluminate ( $C_4A_3S$ ); e) Euhedral, subhedral and anhedral calcium sulfoaluminate grains and belite grains surrounded by calcium sulfoaluminate; f) Ferrite ( $C_4AF$ ) as an interstitial phase; g) periclase (M); h) Elongated gehlenite crystals ( $C_2AS$ ); i) Mayenite ( $C_{12}A_7$ ) as a dark interstitial phase between grains of calcium sulfoaluminate.

surrounded smaller belite grains (Fig. 5e).

Ferrite (Fig. 5c) most commonly appeared as the interstitial phase and anhedral filled the area as above between the belite and calcium sulfoaluminate grains (Fig. 5 e, f). Moreover, the interstitial ferrite, with a diameter of approximately 15  $\mu m$ , was concentrated in individual areas (Fig. 5f). Ferrite crystals up to 6  $\mu m$  in length appeared in nests of up to 25  $\mu m$  long (Fig. 5g), which made KBA2 less homogeneous than KBA1. The fact that the brightness of the phases observed in BSE analysis is proportional to their mean atomic weight can be used for the assessment of the iron content of the ferrite phase [42]. Consequently, in BSE mode ferrites with a high Fe content are brighter than ferrites with lower Fe contents [42]. In KBA2 the interstitial ferrite phase (Fig. 5c, d, e, f, h, i) was brighter than the ferrite crystal nests (Fig. 5g), which could indicate that the ferrite crystals contained less iron than the interstitial ferrite phase, as the ferrite solid solution was trending towards perovskite.

Periclase formed between the belite and calcium sulfoaluminate phase, as subhedral crystals approximately 2  $\mu m$  in length (Fig. 5h). Mayenite appeared between the calcium sulfoaluminate grains (Fig. 5i) and was more common in KBA2 than in KBA1.

In addition to the difference in the proportions of belite and calcium sulfoaluminate between the two clinkers, the belite and calcium sulfoaluminate formed larger grains in KBA1 compared to in KBA2. On the other hand the contact area between the belite grains was generally larger in KBA2 than in KBA1, where neck boundaries were common. The calcium sulfoaluminate in KBA1 mostly appeared as individual grains, while in KBA2 it was concentrated in groups. In KBA1 ferrite presented only as an interstitial phase, while in KBA2 it also formed crystals, concentrated in nests. With respect to the minor phases periclase was evident in both clinkers in similar proportions, while gehlenite was

found only in KBA1. In KBA2 the dominant minor phase was mayenite, which was barely evident in KBA2.

### 3.2.3. The incorporation of minor ions

Fig. 6 shows the elemental distribution of KBA1 (a) and KBA2 (b) sintered at 1300 °C, as revealed by EDS analysis (SEM statistics).

With regard to the major clinker phases, belite, an analogue of the naturally occurring mineral larnite, incorporated Al and Fe in both types of clinker, followed by Mg, S and Ti in KBA1, and S, Ti and Mg in KBA2. This is consistent with the findings that Si can be replaced by other multivalent ions [51,69]. Moreover, in both clinkers belite also incorporated some Na and K, which can substitute Ca in its crystal structure [20,29,70].

The calcium sulfoaluminate in KBA1 and KBA2 also exhibited some Si, Fe, and Ti. The calcium sulfoaluminate could, however, contain some Si, as Al did not replace all of the Si in the sodalite solid solution [13,15]. Moreover, its structure commonly incorporates some Fe and Ti [20]. Some Mg was also detected, which was attributed to the replacement of Ca in the calcium sulfoaluminate structure [20]. In both clinkers the calcium sulfoaluminate also incorporated Na and K, which can be presented in its sodalite type structure [32].

Furthermore, the ferrite in KBA1 and KBA2 incorporated Si, Ti and S. In KBA2 the amount of Ti was greater than S, while in KBA1 the amount of Ti and S were approximately the same. It has been reported that Si and S can substitute Al and Fe in the alumina–ferrite phase [20,71]. In both clinkers calcium sulfoaluminate also included Na and K.

The values of the minor elements listed above decrease from left to right. A clear difference was evident between KBA1 and KBA2, especially in the Ti enrichment of the clinker phases. Belite, calcium sulfoaluminate and ferrite incorporated more Ti in KBA2 compared to

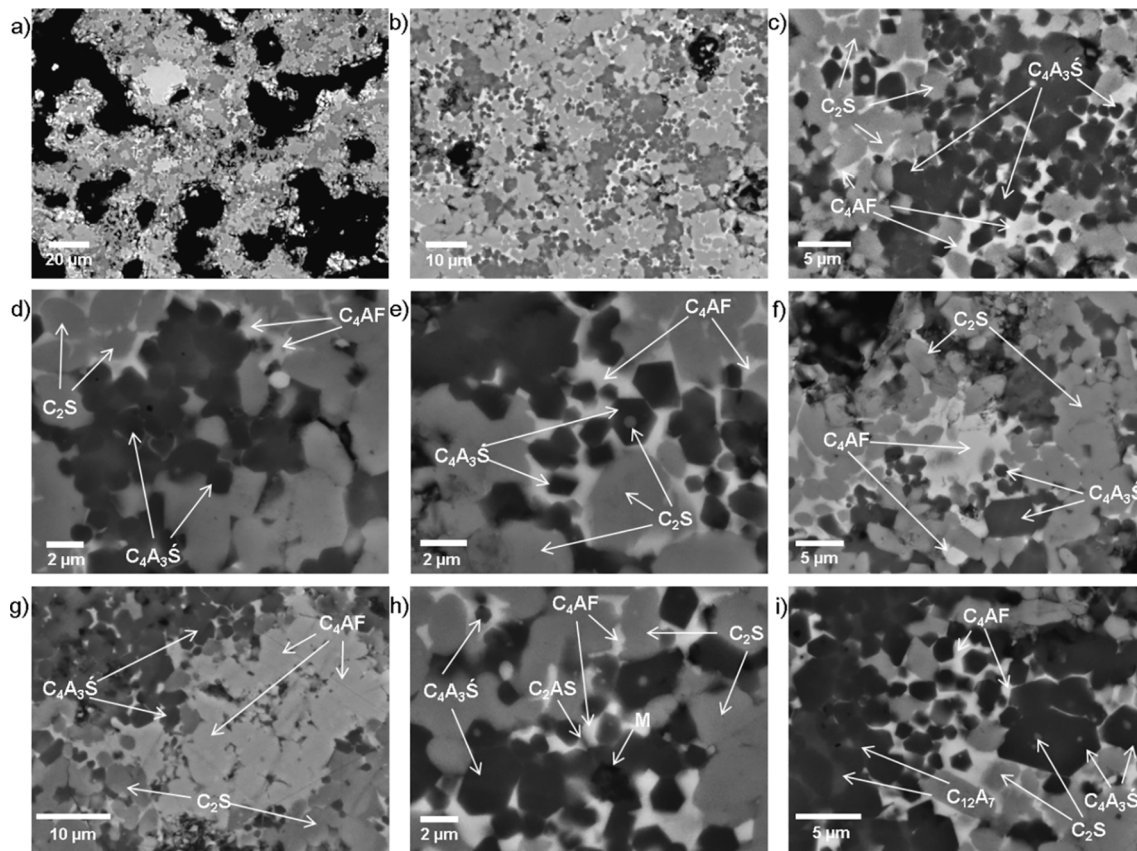


**Fig. 5.** General microstructure (a–c) and microstructural details from KBA2 sintered at 1300 °C: d) Belite ( $C_2S$ ) grains with “neck boundaries” and belite enclosed in calcium sulfoaluminate ( $C_4A_3S$ ); e) Euhedral, subhedral and anhedral grains of calcium sulfoaluminate and belite grains surrounded by calcium sulfoaluminate; f) Ferrite ( $C_4AF$ ) as an interstitial phase; g) Nest of ferrite crystals; h) Periclase (M) and single elongated gehlenite ( $C_2AS$ ) crystals in the ferrite interstitial phase; i) Mayenite ( $C_{12}A_7$ ) as the dark interstitial phase between grains of calcium sulfoaluminate.

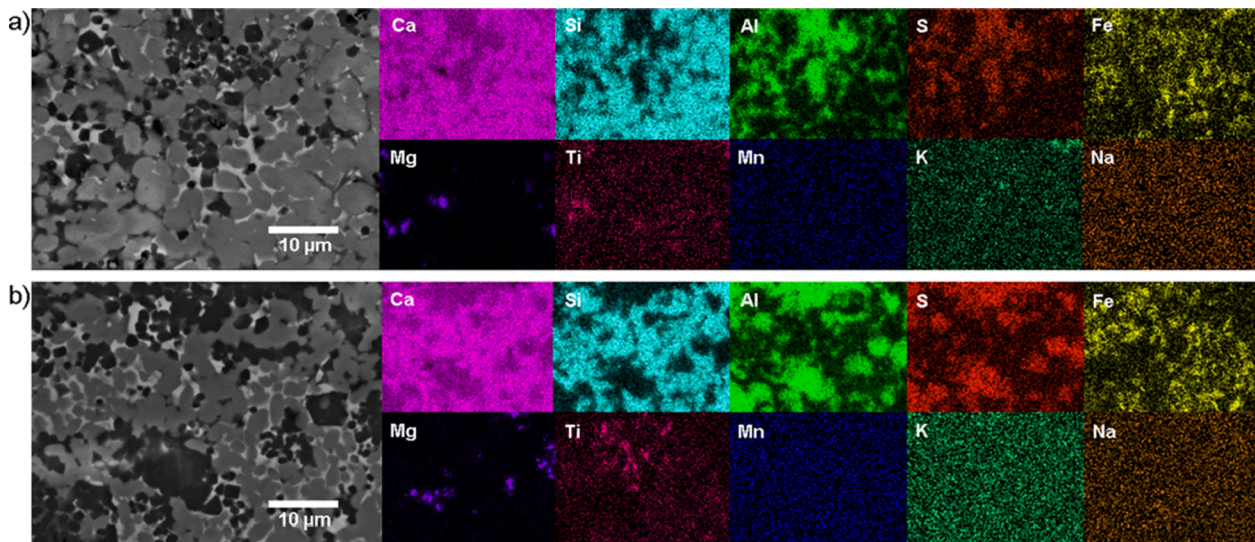


**Fig. 6.** Elemental EDS maps for KBA1 (a) and KBA2 (b) sintered at 1300 °C.

KBA1, which can be explained by the higher Ti-rich bauxite content of the KBA2 raw mixture (Table 1).

Fig. 7 (a–d) shows variations in the chemical composition of the calcium sulfoaluminate phase, the main early age hydration phase of the BCSA clinkers, as determined by EDS analysis. As seen from Fig. 7a, Si was negatively correlated with Al in the calcium sulfoaluminate of both types of clinker, indicating the substitution of Si with Al in the sodalite

solid solution [77].

Calcium sulfoaluminate as sodalite can have Si/Al ratios ranging from zero, for a pure alumina framework, such as ye’elimite, to  $\infty$ , for a pure silica one [78]. Its crystalline structure accepts noticeable amounts of  $Fe^{+3}$  instead of  $Al^{+3}$  forming solid solution. This indicates that Si was a remnant from the early stages of the sodalite solid solution system [77]. The presence of Si in the calcium sulfoaluminate phase has,

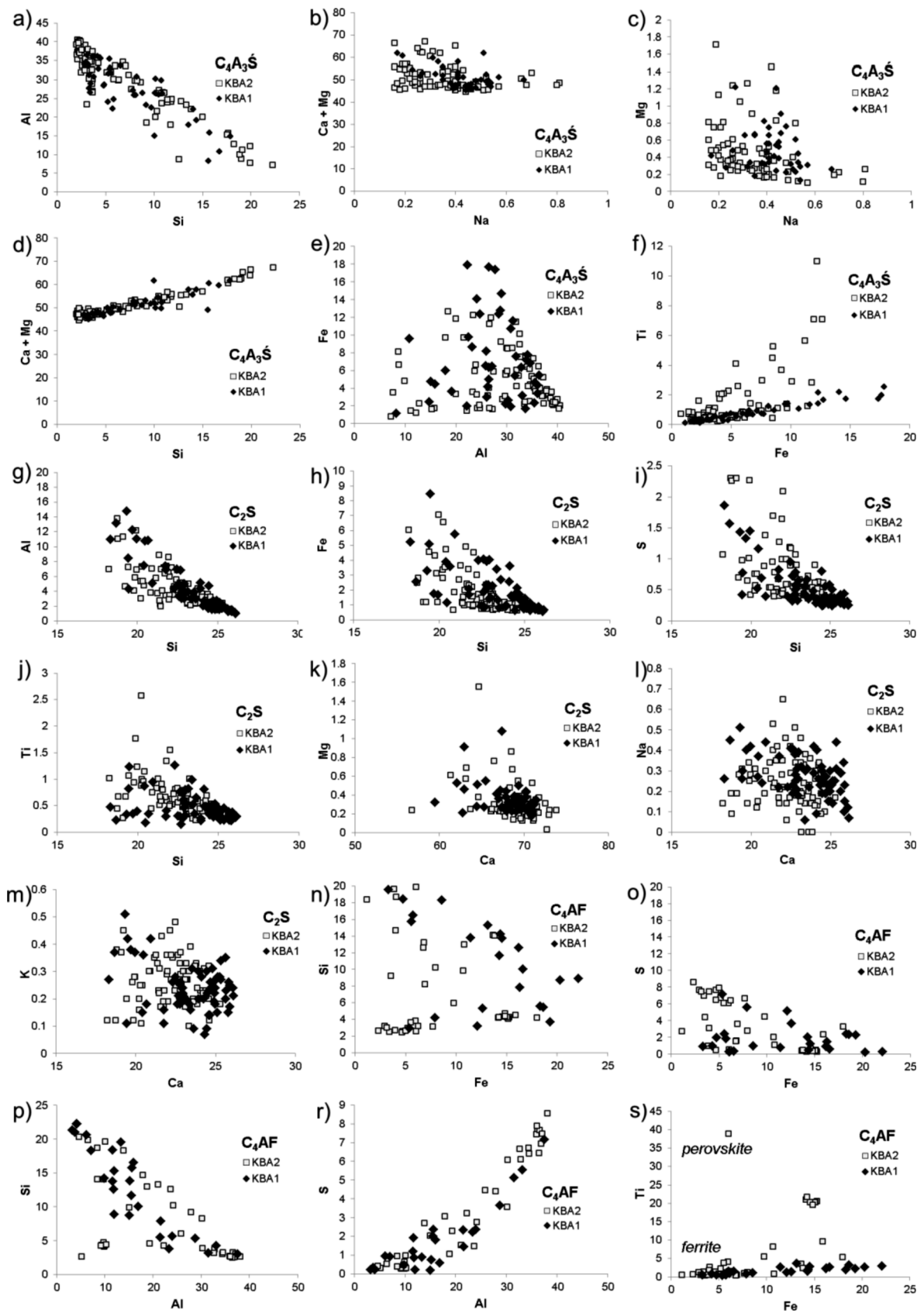


Fig. 7. Comparison of the composition of KBA1 and KBA2, as determined by EDS analysis (weight %), with respect to the following main hydraulic clinker phases: calcium sulfoaluminate (a–f), belite (g–m) and ferrite (n–s).

however, already been reported [8,35]. Furthermore, it has been shown that Na is substituted by Ca in the calcium sulfoaluminate solid solution [31]. As indicated in Fig. 7b, Na was replaced by Ca and Mg in both KBA1 and KBA2, while Mg showed a similar trend as the sum of Ca and Mg (Fig. 7c). The sum of Ca and Mg was positively correlated to Si in both KBA1 and KBA2 (Fig. 7d), which suggests that Ca and Mg were embedded in the calcium sulfoaluminate simultaneously with Si (Fig. 7a). Although in theory Fe is substituted for Al in the calcium sulfoaluminate solid solution [31], Fe and Al seemed not to be correlated in the samples studied (Fig. 7e). On the other hand, Fe and Ti showed a clear positive correlation in KBA1 (Fig. 7f), indicating that Ti did not replace Fe but that they were simultaneously incorporated into the calcium sulfoaluminate structure. The Ti content was higher in KBA2 than in KBA1, but the values were scattered, with a less clear trend than was seen in KBA1 (Fig. 7f).

Belite solid solution represents the main late-stage hydration phase of BCSA clinkers and enables the substitution of Ca with univalent/bivalent ions, such as Mg or alkalis, and the substitution of Si with multivalent ions such as Al, Fe, Ti, and S [69]. Fig. 7 (g-m) shows variations in the chemical composition of the belite phase, as determined by EDS analysis. In belites, Si was negatively correlated with Al (Fig. 7g), Fe (Fig. 7h), S (Fig. 7i) and Ti (Fig. 7j) in both KBA1 and KBA2, indicating the substitution of Si with Al, Fe, S and Ti in the belite solid solution [14]. Similarly, Ca showed a negative correlation with Mg and alkalis (Fig. 7k-m), confirming this substitution.

The ferrite phase has a perovskite type structure, which allows the incorporation of a large amount of foreign elements [71]. The substitution of Si and S with Fe or Al has been reported previously [71]. Si and S are negatively correlated with Fe in both KBA1 and KBA2, although the trend is scattered. Si shows a clear negative correlation with Al (Fig. 7p), indicating the substitution of Al with Si in ferrite in both types of clinker. On the other hand, in both clinkers S shows a clear positive correlation with Al (Fig. 7r), which could indicate that S was embedded in the ferrite simultaneously with Al. It has been reported that Ti in the ferrite phase primarily substitutes at octahedral sites, replacing Fe [14]. In both KBA1 and KBA2, however, a positive correlation between Ti and Fe was determined for the ferrite phase, indicating that Ti did not substitute Fe in the ferrite phase of either KBA1 or KBA2 (Fig. 7u). There was also a clear difference between the ferrite phase composition of the two clinkers, with more Ti incorporated in the ferrite phase of KBA2 compared to KBA1, and a tendency towards a perovskite composition in the former (Fig. 7s).

The most Ti was, however, incorporated into the ferrite phase. As an artificial equivalent of the natural mineral brownmillerite, ferrite has a perovskite-like structure that enables various cation substitutions [72]. Several studies have demonstrated the possible existence of the perovskite-brownmillerite pseudobinary series [59–62]. Ti is one of the most common minor elements, which is often introduced to the cement kilns by industrial waste. Ti is usually present in OPC clinker raw material in an amount of up to 1 wt% [73], but the same amount of Ti has been documented in BCSA clinkers [74]. The presence of Ti in the clinker raw mixture, even in small quantities, significantly improves its hydraulic properties [75] through the substitution of Si with Ti in the ferrite crystal lattice [76]. X-ray powder diffraction results showed the presence of perovskite in both KBA1 and KBA2. Moreover, nests of ferrite crystals, which were found in KBA2 and belong to the perovskite-type of the ferrite phase, were enriched by Ti as shown by EDS analysis. It is evident from Fig. 6 that the least amount of Ti was incorporated into the calcium sulfoaluminate phase.

Higher amounts of Mg were identified in KBA1 due to the higher amount of Mg-rich flysch in the raw mixture (Table 1 and 2). According to Rietveld analysis and SEM/BSE observations, the amount of periclase in KBA1 did not increase. The excess Mg in KBA1 was, however, documented in the belite, calcium sulfoaluminate and ferrite. Alkalis were identified in all phases in both KBA1 and KBA2. KBA1 incorporated more Na than KBA2 (Fig. 7b), however, which can be attributed to the

higher flysch content in KBA1 compared to in KBA2 (Table 1). Similar to Na, higher amounts of K were detected in KBA1 compared to KBA2, corresponding to the higher flysch content in the KBA1 mixture (Table 1).

### 3.3. Isothermal calorimetry

The reactivity of the KBA1 and KBA2 clinkers, sintered at 1200 °C, 1250 °C and 1300 °C without the addition of gypsum, was studied in order to evaluate the influence of the phase microstructure of the clinker and temperature dependent variations in phase composition on clinker reactivity. Because the addition of gypsum significantly influences hydration kinetics [79], clinker reactivity can be investigated without the addition of a sulfate source [16]. Calcium sulfate controls the ratio of precipitated ettringite to monosulfate, resulting from the hydration of calcium sulfoaluminate. In the absence of sulfate, monosulfate and aluminium hydroxide are formed when calcium sulfoaluminate reacts with water, while in the presence of a source of calcium sulfate the main hydration product is ettringite [70,79,80]. As it is also the main phase hydrating in the early stages, however, the hydration of calcium sulfoaluminate itself is very complex; namely ettringite can act as the main hydration product instead of monosulfate [54,74], while ettringite and monosulfate can also occur together [56,80]. The first dissolution peak is only partly visible due to the external mixing method.

After the initial peak, KBA1 sintered at 1200 °C showed a short dormant period [81] until around 2 h, followed by two main exothermic peaks [21], the first occurring at 3 h and the second one after 6 h of hydration (Fig. 8a). These peaks are probably attributed to the precipitation of monosulfate and amorphous aluminium hydroxide resulting from the hydration of ye'elimite [21,56]. Similar hydration kinetics were seen in the KBA2 sintered at 1200 °C as in the KBA1 sintered at 1200 °C, but KBA2 had a longer dormant period after the initial peak, which lasted until a sample age of around 7 h. The first main hydration peak occurred at 9 h and a second heat flow maximum occurred after 11 h of hydration (Fig. 8a). The appearance of two main exothermic peaks at 1200 °C can be attributed to the slow dissolution kinetics of anhydrite [79] in KBA1 (Table 2), while in KBA2 it could be attributed to the changed dissolution kinetics resulting from the fact that the targeted amount of calcium sulfoaluminate had not yet been reached at 1200 °C (Table 2).

A dormant period was observed in KBA1 sintered at 1250 °C after the initial peak at about 13 h. Consequently, formation of the main hydration peak occurred later, at 23 h. After 46 h of hydration a weak second heat flow maximum was identified (Fig. 8b). The dormant period of KBA2, sintered at 1250 °C, was shorter, lasting until a sample age of about 6 h, while the main hydration peak didn't occur until 18 h (Fig. 8b).

The dormant period of KBA1 sintered at 1300 °C occurred at an intermediate value, lasting until a sample age of about 7 h. The main hydration peak occurred at 24 h (Fig. 8c). The shortest dormant period occurred in KBA2 sintered at 1300 °C, terminating at a sample age of about 3 h. The main hydration peak occurred at 14 h of reaction (Fig. 8c).

The highest total cumulative heat after 72 h was identified in the KBA1 sintered at 1200 °C (138 J/g), while after 72 h the KBA1 sintered at 1250 and 1300 °C both had a total cumulative heat of 123 J/g. Similar to in the KBA1 mixture, in KBA2 the highest total heat flow of hydration value after 72 h (184 J/g) was determined at 1200 °C.

In both KBA1 and KBA2 the reaction of the clinker sintered at 1200 °C yielded the shortest dormant period. The smallest calcium sulfoaluminate grain size, however, as observed by SEM, occurred in the clinkers sintered at 1200 °C, which could lead to the fastest dissolution rate. The wetting time and main hydration peak of KBA1 sintered at 1250 and 1300 °C were similar, but at 1250 °C a second hydration peak occurred, which was not detected at 1300 °C. In KBA2, the sample sintered at 1250 °C reacted faster than the one sintered at 1300 °C.

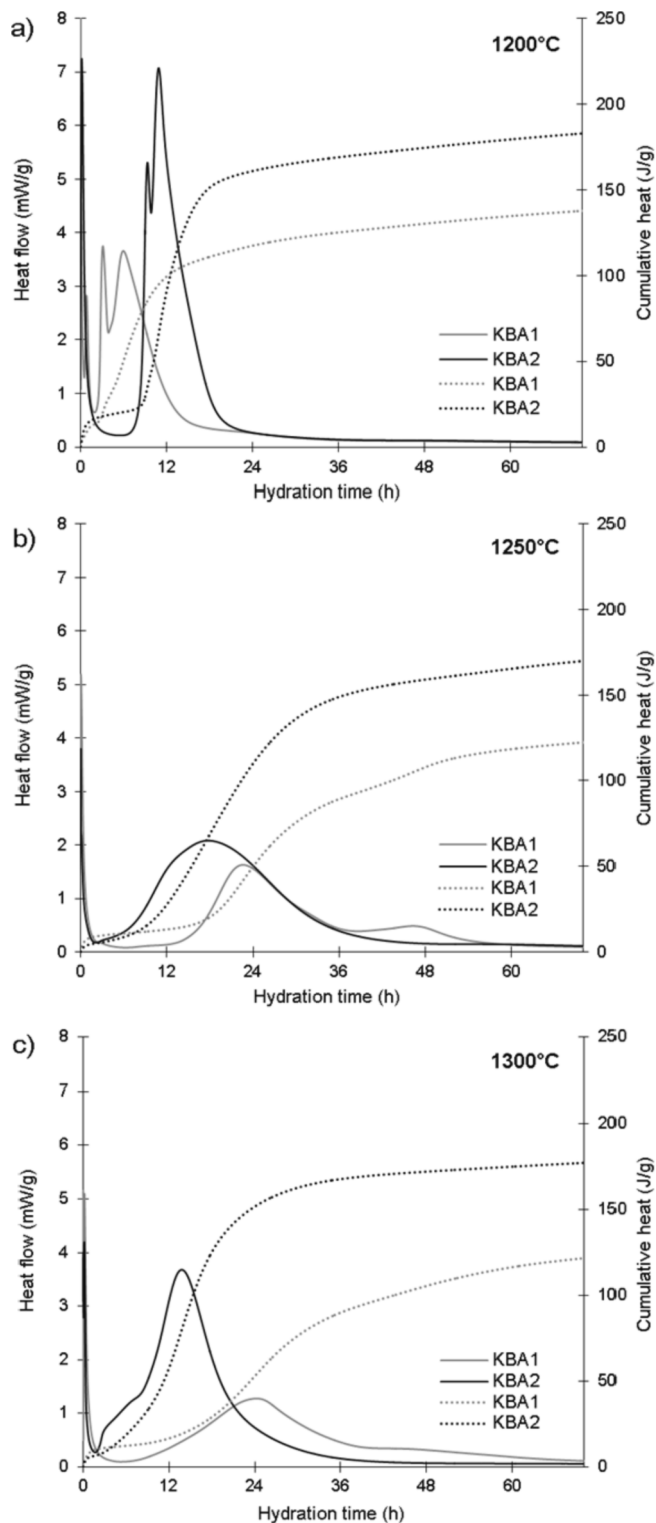


Fig. 8. Heat flow and cumulative heat curves for KBA1 and KBA2 ( $w/c = 0.5$  at  $20\text{ }^{\circ}\text{C}$ ) sintered at  $1200\text{ }^{\circ}\text{C}$  (a),  $1250\text{ }^{\circ}\text{C}$  (b) and  $1300\text{ }^{\circ}\text{C}$  (c).

Comparing the clinkers sintered at  $1200\text{ }^{\circ}\text{C}$ , the hydration of calcium sulfoaluminate was more rapid in KBA1 compared to in KBA2 (Fig. 8a). As both clinkers had a similar Blaine specific surface area (Table 3), the faster early hydration of KBA1 can be attributed to the presence of anhydrite in KBA1, which represented an additional sulfate source to accelerate the formation of monosulfate.

In KBA1 less heat flow was released during the hydration compared

Table 3

The main parameters of the PSD curves, specific density and Blaine SSA.

Sintering T ( $^{\circ}\text{C}$ )	1200		1250		1300	
	KBA1	KBA2	KBA1	KBA2	KBA1	KBA2
Raw mixture						
PSD $d_{10}$ ( $\mu\text{m}$ )	1.42	2.87	2.44	3.58	3.18	3.74
PSD $d_{50}$ ( $\mu\text{m}$ )	8.99	13.52	18.39	17.83	39.38	29.87
PSD $d_{90}$ ( $\mu\text{m}$ )	27.09	34.11	71.23	46.58	104.73	82.46
Specific density ( $\text{g}/\text{cm}^3$ )	3.23	3.11	3.23	3.11	3.23	3.08
Blaine SSA ( $\text{cm}^2/\text{g}$ )	3827	3743	2860	3032	2237	2417

to in KBA2 at all three sintering temperatures. Moreover, after 72 days of hydration KBA2 had a higher total cumulative heat than KBA1, again at all sintering temperatures (Fig. 8). This indicates that KBA1 was generally less reactive than KBA2, as is consistent with the targeted phase composition; KBA2 contains 35 wt% of calcium sulfoaluminate, the most reactive early age hydration phase, compared to only 20 wt% of this phase in KBA1 (Table 1). Another parameter which could contribute to the higher reactivity of KBA2 is the calcium sulfoaluminate grain size, since a decrease in the grain diameter has been proven to improve the reactivity of the clinker phases. Namely, the proportion of the smallest grain sizes ( $0\text{--}1\text{ }\mu\text{m}$ ) in the calcium sulfoaluminate was higher in KBA2 than in KBA1 (Fig. 3). Moreover, EDS analysis revealed that the calcium sulfoaluminate incorporated more Ti in KBA2 than in KBA1 (data measured on clinkers sintered at  $1300\text{ }^{\circ}\text{C}$ ). Given that Ti can promote the hydraulic activity of the clinker phases [75], a higher Ti content in KBA2 could also contribute to a higher reactivity. The latter was studied for the OPC system, however, since data regarding the incorporation of Ti in calcium sulfoaluminate are not available. Finally, a lower reactivity of KBA1 could also be partly explained by the greater formation of nonreactive gehlenite in KBA2 compared to KBA1.

In both KBA1 and KBA2 the Blaine specific surface area decreased with an increase in sintering temperature (Table 3), which was associated with densification of the microstructure [82], as was also evident by SEM/EDS analysis (Fig. 2). Comparing KBA1 and KBA2 sintered at the same temperatures, the specific surface area of KBA2 was slightly higher, which could be attributed to the higher calcium sulfoaluminate content of the KBA2. The exception was at  $1200\text{ }^{\circ}\text{C}$ , where KBA1 had a slightly higher specific surface area than KBA2 (Table 3). The differences in Blaine specific surface area between KBA1 and KBA2 at the same sintering temperature are small ( $84\text{ cm}^2/\text{g}$  at  $1200\text{ }^{\circ}\text{C}$ ,  $172\text{ cm}^2/\text{g}$  at  $1250\text{ }^{\circ}\text{C}$  and  $180\text{ cm}^2/\text{g}$  at  $1300\text{ }^{\circ}\text{C}$ ) and should therefore not significantly contribute to clinker reactivity (Table 3). The overall PSD of KBA1 sintered at  $1200$ ,  $1250$  and  $1300\text{ }^{\circ}\text{C}$  showed similar unimodal distributions (Fig. 9a), with a main peak at around  $2\text{ }\mu\text{m}$ , while the amount of coarse fraction increased by increasing the temperature (Table 3), as a consequence of the decreased clinker grindability [82]. Namely, at a higher sintering temperature, the microstructure is densified [83] and the grains are larger. The density distribution was less uniform in KBA2; at  $1200\text{ }^{\circ}\text{C}$  and  $1250\text{ }^{\circ}\text{C}$  it was bimodal with peaks at around  $2\text{ }\mu\text{m}$  and  $8\text{ }\mu\text{m}$ , while at  $1300\text{ }^{\circ}\text{C}$  it became a unimodal curve with a main distribution peak at around  $2\text{ }\mu\text{m}$  (Fig. 9b). Similar to KBA1, the increase in coarse fraction and decrease in the finest fraction in line with an increase in sintering temperature was also evident in KBA2 (Table 3). The clinkers sintered at  $1200\text{ }^{\circ}\text{C}$ , however, reacted faster and reached a higher cumulative heat compared to the clinkers sintered at higher temperatures, which can mostly be attributed to the effects of particle size distribution and specific surface area. KBA2 clinkers were finer than KBA1 ( $d$  values in Table 3), probably due to the lower belite content, which contributes to easier grinding.

Development of good mechanical strength and durability properties in cement pastes commonly requires the addition of a sulfate source [81]. The hydration of cements containing calcium sulfoaluminate is a complex process that depends on various parameters [21]. The addition of gypsum, however, generally accelerates the hydration of calcium

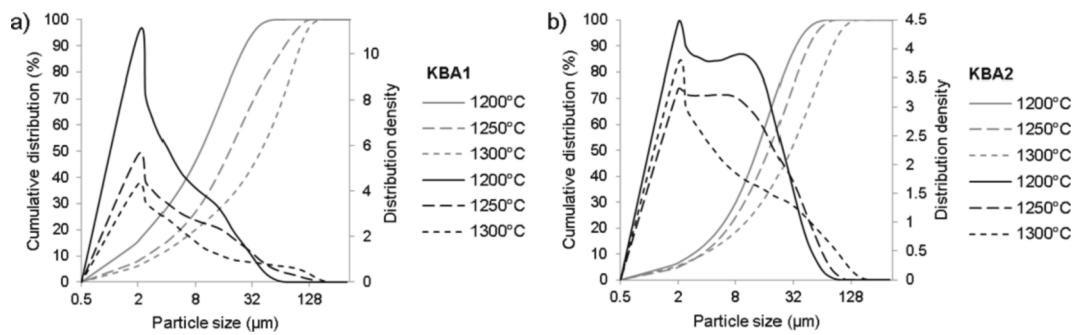


**Fig. 9.** Cumulative distribution (% passing, based on volume) and density distribution (derivatives of cumulative distribution, based on volume) of clinkers KBA1 (a) and KBA2 (b).

sulfoaluminate [54]. For example, in the clinker with the KBA1 phase composition, sintered at 1250 °C and blended with 20.3 wt% gypsum, the precipitation of ettringite occurred at around 3 h [84,85], while in the pure clinker this only occurred at about 13 h of hydration (Fig. 8b). At 7 days of hydration cement pastes made with the KBA1 clinker (20.3 wt% of gypsum,  $w/c = 0.5$ ) and sintered at 1250 °C reached a compressive strength of around 13 N/mm<sup>2</sup> [84], while the strength of the same clinker sintered at 1300 °C ranged from 11.5 to 18.8 N/mm<sup>2</sup> [86], depending on the clinker cooling method employed and its consequent microstructure. The compressive strength of the KBA1 cement pastes ( $w/c = 0.5$ ) sintered at 1250 °C and blended with 20.3 wt % gypsum was fairly constant until 28 days of hydration (approx. 13 N/mm<sup>2</sup>), whereas a significant increase was evident after 90 days of hydration, with the compressive strength rising to around 22 N/mm<sup>2</sup> [84].

#### 4. Conclusions

The aim of this paper was to investigate the incorporation mechanisms of bottom ash into BCSA clinkers. The microstructures of two different BCSA cement clinkers (with targeted phase compositions of 65 wt% belite, 20 wt% calcium sulfoaluminate, 10 wt% ferrite (KBA1) and 50 wt% belite, 35 wt% calcium sulfoaluminate and 10 wt% ferrite (KBA2)) sintered at 1200 °C, 1250 °C and 1300 °C were studied. Both mixtures incorporated approximately 9 wt% bottom ash.

The targeted phase composition of KBA1 was reached at a temperature 50 °C lower than KBA2, which could be related to the higher alkali content in the raw mix. With respect to the minor phases, periclase, perovskite, arcanite and aphtialite were presented in both types of clinker. Gehlenite, some mayenite,  $\gamma$ -belite and anhydrite were also detected in KBA1, while in KBA2 mayenite and some free lime were present. The absence of  $\gamma$ -belite in KBA2 can be attributed to the higher Ti content in the raw mix, which stabilized the  $\beta$ -belite.

Clinkers showed a fine-grained texture with a decrease in porosity occurring with an increase in sintering temperature. Belite grains with unclear boundaries were already evident at 1200 °C and with an increase in temperature, their form changed from being mostly rounded anhedral/subhedral to subangular, subrounded quadrangular and hexagonal subhedral. Calcium sulfoaluminate formed an interstitial phase between the belite grains at 1200 and 1250 °C and only at 1300 °C developed subangular to quadrangular and hexagonal subhedral to euhedral grains. The grain size of belite increased with an increase in sintering temperature. Ferrite formed an interstitial phase at all sintering temperatures in both clinker phase compositions. At 1300 °C gehlenite was clearly evident on SEM images in KBA1, while it was not present in KBA2. On the other hand, mayenite was clearly present in KBA2, but was barely detectable in KBA1.

Some Si presented in calcium sulfoaluminate as a result of the incomplete substitution of Si by Al in the sodalite solid solution. Na was substituted by Ca and Mg, while Fe and Ti became incorporated into the sodalite structure, without replacing Al. In belite Si was replaced by Al,

Fe, S and Ti, while Ca was replaced by Mg, Na and K. In ferrite Al was substituted with Si, while S was simultaneously incorporated into the ferrite phase by Al. Ti was incorporated into ferrite without the replacement of Fe. The mechanism of incorporation of minor elements into the main clinker phases was similar in both KBA1 and KBA2. As ferrite incorporated higher amounts of Ti in KBA2, however, the solid solution trended towards a perovskite composition. In KBA1 the main clinker phases incorporated more alkalis and Mg than in the KBA2 clinker, which was attributed to the higher flysch content of KBA1.

The variation in sintering temperature influenced the clinker phase composition and contributed to clinker reactivity, as was evident by isothermal calorimetry. Due to its lower calcium sulfoaluminate content KBA1 was generally less reactive than KBA2. The clinkers sintered at 1200 °C were the most reactive. The presence of anhydrite in KBA1, and the changed dissolution kinetics in KBA2 at 1200 °C, due to the fact that the targeted amount of major clinker phases had not been reached, resulted in two main exothermic peaks. In KBA1 1.2% of anhydrite formed at 1200 °C, significantly accelerating early hydration compared to KBA2, in which no anhydrite presented at the same temperature.

A second hydration peak occurred at 1250 °C in KBA1, which was mainly attributed to the formation of monosulfate together with aluminium hydroxide. Clinker reactivity was, however, additionally influenced by the particle size distribution and specific surface area, as in both phase compositions the most reactive clinkers were those sintered at 1200 °C. In KBA2, the clinker sintered at 1250 °C was more reactive than that sintered at 1300 °C.

In this study bottom ash was shown to be an adequate raw material for the synthesis of BCSA clinkers. The main clinker phases of the belite-sulfoaluminate clinker enabled the incorporation of various minor elements, however, which influenced the clinker's properties. This can be controlled by the appropriate selection of basic raw materials (limestone or siliciclastic rocks). Sintering temperature, on the other hand, highly affected the microstructure and grindability of the clinker, which resulted in a decrease in clinker reactivity with an increase in sintering temperature. Since BCSA clinkers are very sensitive to impurities derived from the raw mixture, which can strongly influence the hydration behaviour of the clinker, further studies are necessary before the wider production of BCSA clinkers from secondary raw materials can be implemented. As such, our results offer an important starting point for future research.

#### CRediT authorship contribution statement

**Lea Žibret:** Conceptualization, Methodology, Investigation, Writing – original draft. **Andrej Ipavec:** Conceptualization, Methodology, Writing – original draft, Supervision. **Sabina Dolenc:** Conceptualization, Methodology, Writing – original draft, Supervision.

## Declaration of Competing Interest

The authors declare that they have no known competing financial interests or personal relationships that could have appeared to influence the work reported in this paper.

## Acknowledgements

Project No. C3330-17-529035 “Raziskovalci-2.0-ZAG-529035” was granted by the Ministry of Education, Science and Sport of the Republic of Slovenia. The investment is co-financed by the Republic of Slovenia, Ministry of Education, Science and Sport and the European Regional Development Fund. The authors acknowledge financial support from the Slovenian Research Agency (research core funding No. P2-0273). We would also like to thank to Prof. Matej Dolenc for advice on describing clinker phase morphology and to three anonymous reviewers for their valuable comments which helped to improve the manuscript.

## References

- E. Gartner, Industrially interesting approaches to “low CO<sub>2</sub>” cements, *Cem. Concr. Res.* 34 (9) (2004) 1489–1498, <https://doi.org/10.1016/j.cemconres.2004.01.021>.
- E. Gartner, T. Sui, Alternative cement clinkers, *Cem. Concr. Res.* 114 (2018) 27–39, <https://doi.org/10.1016/j.cemconres.2017.02.002>.
- J.S. Damtoft, J. Lukasik, D. Herfort, D. Sorrentino, E.M. Gartner, Sustainable development and climate change initiatives, *Cem. Concr. Res.* 38 (2) (2008) 115–127, <https://doi.org/10.1016/j.cemconres.2007.09.008>.
- B. Ma, X. Li, Y. Mao, X. Shen, Synthesis and characterization of high belite sulfoaluminate cement through rich alumina fly ash and desulfurization gypsum, *Ceram. – Silik.* 57 (2013) 7–13.
- R.I. Iacobescu, Y. Pontikes, D. Koumpouri, G.N. Angelopolous, Synthesis, characterization and properties of calcium ferroaluminate belite cements produced with electric arc furnace steel slag as raw material, *Cem. Concr. Compos.* 44 (2013) 1–8, <https://doi.org/10.1016/j.cemconcomp.2013.08.002>.
- W. Wang, X. Wang, J. Zhu, P. Wang, C. Ma, Experimental investigation and modelling of sulfoaluminate cement preparation using desulfurization gypsum and red mud, *Ind. Eng. Chem. Res.* 52 (2013) 1261–1226, <https://doi.org/10.1021/ie301364c>.
- V. Isteri, K. Ohenoja, T. Hanein, H. Kinoshita, P. Tanskanen, M. Illikainen, T. Fabritius, Production and properties of ferrite-rich CSAB cement from metallurgical industry residues, *Sci. Total Environ.* 712 (2020).
- Ö. Andac, F.P. Glasser, Microstructure and microchemistry of calcium sulfoaluminate cement, *Mat. Res. Soc. Symp. Proc.* 370 (1995) 135–142.
- C.J. Chan, W.M. Kriven, J.F. Young, Physical stabilization of the  $\beta$   $\gamma$  Transformation in Dicalcium silicate, *J. Am. Ceram. Soc.* 75 (1992) 1621–1627, <https://doi.org/10.1111/j.1151-2916.1992.tb04234.x>.
- W. Dienemann, D. Schmitt, F. Bullerjahn, M. Ben Haha, Belitecalciumsulfoaluminate-ternesite (BCT)-a new low-carbon clinker technology, *Cem. Int.* 11 (2013) 100–109.
- F. Bullerjahn, D. Schmitt, M. Ben Haha, Effect of raw mix design and clinkering process on the formation and mineralogical composition of (ternesite) belite calcium sulfoaluminate ferrite clinker, *Cem. Concr. Res.* 59 (2014) 87–95, <https://doi.org/10.1016/j.cemconres.2014.02.004>.
- G. Álvarez-Pinazo, A. Cuesta, M. García-Maté, I. Santacruz, E.R. Losilla, A.G.D. la Torre, L. León-Reina, M.A.G. Aranda, Rietveld quantitative phase analysis of Yeelite-containing cements, *Cem. Concr. Res.* 42 (7) (2012) 960–971, <https://doi.org/10.1016/j.cemconres.2012.03.018>.
- A. Cuesta, G. Álvarez-Pinazo, S.G. Sanfélix, I. Pearl, M.A.G. Aranda, Á.G. De la Torre, Hydration mechanisms of two polymorphs of synthetic ye’elinite, *Cem. Concr. Res.* 63 (2014) 127–136, <https://doi.org/10.1016/j.cemconres.2014.05.010>.
- C.W. Hargis, Advances in Sustainable Cements, Doctoral Dissertation of Civil and Environmental Engineering, University of California, Berkeley, 2013.
- A. Cuesta, A.G. De la Torre, E.R. Losilla, V.K. Peterson, P. Rejmak, A. Ayuela, C. Frontera, M.A.G. Aranda, Structure, atomistic simulations, and phase transition of stoichiometric yeelite, *Chem. Mater.* 25 (9) (2013) 1680–1687, <https://doi.org/10.1021/cm400129z>.
- F. Bullerjahn, M. Zajac, M. Ben Haha, CSA raw mix design: Effect on clinker formation and reactivity, *Mater. Struct.* 48 (12) (2015) 3895–3911, <https://doi.org/10.1617/s11527-014-0451-z>.
- T. Hanein, I. Galan, A. Elhoweris, S. Khare, S. Skalamprinos, G. Jen, M. Whittaker, M.S. Imbabi, F.P. Glasser, M.N. Bannerman, Production of belite calcium sulfoaluminate cement using sulfur as a fuel and as a source of clinker sulfur trioxide: pilot kiln trial, *Adv. Cem. Res.* 28 (10) (2016) 643–653, <https://doi.org/10.1680/jadcr.16.00018>.
- I. Galan, T. Hanein, A. Elhoweris, M.N. Bannerman, F.P. Glasser, Phase Compatibility in the System CaO–SiO<sub>2</sub>–Al<sub>2</sub>O<sub>3</sub>–SO<sub>3</sub>–Fe<sub>2</sub>O<sub>3</sub> and the Effect of Partial Pressure on the Phase Stability, *Ind. Eng. Chem. Res.* 56 (9) (2017) 2341–2349, <https://doi.org/10.1021/acs.iecr.6b03470>.
- Y. Takuma, T. Shirasaka, M. Kanaya, K. Kobayashi, S. Uchida, Effect of Reducing the Emissions of CO<sub>2</sub> and the Characters of Clinker in the System C<sub>2</sub>S–C<sub>4</sub>A<sub>3</sub>S–C<sub>4</sub>AF–CS, *J. Ceram. Soc. JPN* 102 (1994) 1115–1121, <https://doi.org/10.2109/jcersj.102.1115>.
- J. Strigáč, M. Palou, J. Kristín, J. Majling, Morphology and Chemical composition of minerals inside the phase assemblage C–C<sub>2</sub>S–C<sub>4</sub>A<sub>3</sub>S–C<sub>4</sub>AF–CS relevant to sulfoaluminate belite cements, *Ceram. – Silik.* 44 (1999) 26–34.
- M. Ben Haha, F. Winnefeld, A. Pisch, Advances in understanding ye’elinite-rich cements, *Cem. Concr. Res.* 123 (2019) 1–20, <https://doi.org/10.1016/j.cemconres.2019.105778>.
- G.Q. Liu, Q.X. Yang, L. Jiang, P. Xue, X.L. Zhang, F.L. Han, Sintering characteristics of BC SAF cement clinker with added wastes from production of manganese and magnesium metals, *Adv. Cem. Res.* 29 (2017) 227–235, <https://doi.org/10.1680/jadcr.16.00035>.
- K. Kolovos, P. Loutsis, S. Tsvivilis, G. Kakali, The effect of foreign ions on the reactivity of the CaO–SiO<sub>2</sub>–Al<sub>2</sub>O<sub>3</sub>–Fe<sub>2</sub>O<sub>3</sub> system. Part I: Anions, *Cem. Concr. Res.* 31 (3) (2001) 425–429, [https://doi.org/10.1016/S0008-8846\(00\)00461-0](https://doi.org/10.1016/S0008-8846(00)00461-0).
- K. Kolovos, S. Tsvivilis, G. Kakali, The effect of foreign ions on the reactivity of the CaO–SiO<sub>2</sub>–Al<sub>2</sub>O<sub>3</sub>–Fe<sub>2</sub>O<sub>3</sub> system. Part II: Cations, *Cem. Concr. Res.* 32 (3) (2002) 463–469, [https://doi.org/10.1016/S0008-8846\(01\)00705-0](https://doi.org/10.1016/S0008-8846(01)00705-0).
- K. Kolovos, S. Tsvivilis, G. Kakali, SEM examination of clinkers containing foreign elements, *Cem. Concr. Compos.* 27 (2) (2005) 163–170, <https://doi.org/10.1016/j.cemconcomp.2004.02.003>.
- P.K. Mehta, Investigations on energy-saving cements, *World Cem. Technol.* 11 (1980) 166–177.
- P. Arjunan, M.R. Silsbee, D.M. Roy, Sulfoaluminate-belite cement from low-calcium fly ash and sulfur-rich and other industrial by-products, *Cem. Concr. Res.* 29 (1999) 1305–1311, [https://doi.org/10.1016/S0008-8846\(99\)00072-1](https://doi.org/10.1016/S0008-8846(99)00072-1).
- Y.-M. Kim, S.-H. Hong, Influence of minor ions on the stability and hydration rates of  $\beta$ -dicalcium silicate, *J. Am. Ceram. Soc.* 87 (5) (2004) 900–905, <https://doi.org/10.1111/j.1551-2916.2004.00900.x>.
- A. Cuesta, A. Ayuela, M.A.G. Aranda, Belite cements and their activation, *Cem. Concr. Res.* 140 (2021) 106319, <https://doi.org/10.1016/j.cemconres.2020.106319>.
- T. Staněk, P. Sulovský, Dicalcium silicate doped with sulfur, *Adv. Cem. Res.* 24 (4) (2012) 233–238, <https://doi.org/10.1680/adcr.11.00021>.
- H. Manzano, E. Durgum, M.J. Abdolhosseini Qomi, F.-J. Ulm, R.J.M. Pellenq, J. C. Grossman, Impact of chemical impurities on the crystalline cement clinker phases determined by atomistic simulations, *Cryst. Growth Des.* 11 (7) (2011) 2964–2972, <https://doi.org/10.1021/cg200212c>.
- O. Andac, F.P. Glasser, Polymorphism of calcium sulfoaluminate (Ca<sub>2</sub>Al<sub>6</sub>O<sub>16</sub>–SO<sub>3</sub>) and its solid solutions, *Adv. Cem. Res.* 6 (22) (1994) 57–60.
- M. Idrissi, A. Diouri, D. Damidot, J.M. Greneche, M.A. Talbi, M. Taibi, Characterisation of iron inclusion during the formation of calcium sulfoaluminate phase, *Cem. Concr. Res.* 40 (8) (2010) 1314–1319, <https://doi.org/10.1016/j.cemconres.2010.02.009>.
- Y. Li, X. Liu, X. Niu, L. Song, Influence of minor oxides on formation and decomposition of mineral calcium sulfoaluminate (3CaO·3Al<sub>2</sub>O<sub>3</sub>·CaSO<sub>4</sub>), *Mater. Res. Innov.* 11 (2) (2007) 92–94, <https://doi.org/10.1179/143307507X196644>.
- A. Berrio, C. Rodríguez, J. Tobon, Effect of Al<sub>2</sub>O<sub>3</sub>/SiO<sub>2</sub> ratio on ye’elinite production on CSA cement, *Constr. Build. Mater.* 168 (2018) 512–521, <https://doi.org/10.1016/j.conbuildmat.2018.02.153>.
- I.A. Chen, M.C.G. Juenger, Synthesis and hydration of calcium sulfoaluminate-belite cements with varied phase compositions, *J. Mater. Sci.* 46 (8) (2011) 2568–2577, <https://doi.org/10.1007/s10853-010-5109-9>.
- K. Morsli, Á.G. de la Torre, M. Zahir, M.A.G. Aranda, Mineralogical phase analysis of alkali and sulfate bearing belite rich laboratory clinkers, *Cem. Concr. Res.* 37 (5) (2007) 639–646, <https://doi.org/10.1016/j.cemconres.2007.01.012>.
- A. Cuesta, E.R. Losilla, M.A.G. Aranda, J. Sanz, Á.G. De la Torre, Reactive belite stabilization mechanisms by boron-bearing dopants, *Cem. Concr. Res.* 42 (4) (2012) 598–606, <https://doi.org/10.1016/j.cemconres.2012.01.006>.
- C. Argiz, M.A. Sanjuán, E. Menéndez, Coal Bottom Ash for Portland Cement Production, *Adv. Mater. Sci. J. Eng.* 2017 (2017) 1–7, <https://doi.org/10.1155/2017/6068286>.
- AMERICAN COAL ASSOCIATION, 2019: <https://aca-usa.org/wp-content/uploads/coal-combustion-products-use/2019-Survey-Results.pdf> (26.7.2021).
- M. Adama, R. Esena, B. Fosu-Mensah, D. Yirenya-Tawiah, Heavy Metal Contamination of Soils around a Hospital Waste Incinerator Bottom Ash Dumps Site, *J. Environ. Publ. Heal.* 2016 (2016) 1–6, <https://doi.org/10.1155/2016/8926453>.
- [http://www.ecoba.com/evjm\\_media/ccps/ECO\\_stat\\_2016\\_EU15\\_tab.pdf](http://www.ecoba.com/evjm_media/ccps/ECO_stat_2016_EU15_tab.pdf) (26.7.2021).
- M.L.D. Jayaranjan, E.D. van Hullebusch, A.P. Annachhatre, Reuse options for coal fi red power plant bottom ash and fly ash, *Rev. Environ. Sci. Bio.* 13 (4) (2014) 467–486, <https://doi.org/10.1007/s1157-014-9336-4>.
- I.A. Chen, M.C.G. Juenger, Incorporation of coal combustion residuals into calcium sulfoaluminate-belite cement clinkers, *Cement Concrete Res.* 34 (8) (2012) 893–902, <https://doi.org/10.1016/j.cemconcomp.2012.04.006>.
- D. Su, G. Yue, Q. Li, Y. Guo, S. Gao, L. Wang, Research on the preparation and properties of high belite sulfoaluminate cement (HBSAC) based on various industrial solid wastes, *Materials.* 19 (2019) 1510, <https://doi.org/10.3390/ma12091510>.
- S. Kramar, L. Žibret, E. Fidanchevska, V. Jovanov, B. Angjusheva, V. Ducman, Use of fly ash and phosphogypsum for the synthesis of belite-sulfoaluminate clinker, *Mater. Construcc.* 69 (2019) 1–12, <https://doi.org/10.3989/mc.2019.11617>.

- [47] E. Aydin, Novel coal bottom ash waste composites for sustainable construction, *Constr. Build. Mater.* 124 (2016) 582–588, <https://doi.org/10.1016/j.conbuildmat.2016.07.142>.
- [48] A. Rungchet, C.S. Poon, P. Chindaprasit, K. Pimraksa, Synthesis of low-temperature calcium sulfoaluminate-belite cements from industrial wastes and their hydration: Comparative studies between lignite fly ash and bottom ash, *Cem. Concr. Compos.* 83 (2017) 10–19, <https://doi.org/10.1016/j.cemconcomp.2017.06.013>.
- [49] S. Buser, Geological map of Slovenia 1: 250 000 (adopted after OGK 1: 100,000 and amended), Geological survey of Slovenia, Ljubljana, 2009.
- [50] J. Majling, J. Strigáč, D.M. Roy, Generalized Bogue computations to forecast the mineralogical composition of sulfoaluminate cements based on fly ashes, *Adv. Cem. Res.* 11 (1) (1999) 27–34.
- [51] S.N. Ghosh, P.B. Rao, A.K. Paul, K. Raina, The Chemistry of Dicalcium Silicate Minerals, *J. Mater. Sci.* 14 (7) (1979) 1554–1566.
- [52] I. Odler, Special Inorganic Cements, E&FN Spon, London, 2000.
- [53] C.W. Hargis, J. Moon, B. Lothenbach, F. Winnefeld, H.-R. Wenk, P.J.M. Monteiro, J. Biernacki, Calcium sulfoaluminate sodalite ( $\text{Ca}_4\text{Al}_6\text{O}_{12}\text{SO}_4$ ) crystal structure evaluation and bulk modulus determination, *J. Am. Ceram. Soc.* 97 (3) (2014) 892–898.
- [54] D. Jansen, A. Spies, J. Neubauer, D. Ectors, F. Goetz-Neunhoffer, Studies on the early hydration of two modifications of ye'elimite with gypsum, *Cem. Concr. Res.* 91 (2017) 106–116, <https://doi.org/10.1016/j.cemconres.2016.11.009>.
- [55] A.G. De la Torre, D. Londono-Zuluaga, J.D. Zea-García, M. García-Maté, G. Álvarez-Pinazo, M.A.G. Aranda, I. Santacruz, A. Cuesta, L. León-Reina, F. Franco, J. I. Tobón, A. Diouri, A. Boukhari, L. Ait Brahim, L. Bahi, N. Khachani, M. Saadi, J. Aride, A. Nounah, X-ray diffraction, cements and environment, three worlds in one, *MATEC Web of Conferences* 149 (2018) 01003, <https://doi.org/10.1051/mateconf/201814901003>.
- [56] F. Bullerjahn, M. Zajac, M. Ben Haha, K.L. Scrivener, Factors influencing the hydration kinetics of ye'elimite; effect of mayenite, *Cem. Concr. Res.* 116 (2019) 113–119, <https://doi.org/10.1016/j.cemconres.2018.10.026>.
- [57] D.H. Lister, F.P. Glasser, Phase relations in the system  $\text{CaO}-\text{Al}_2\text{O}_3-\text{Fe}_2\text{O}_3$ , *Br. Ceram. Soc. Trans.* 66 (1967) 293–306.
- [58] B. Touzo, K.L. Scrivener, F.P. Glasser, Phase compositions and equilibria in the  $\text{CaO}-\text{Al}_2\text{O}_3-\text{Fe}_2\text{O}_3-\text{SO}_3$  system, *Cem. Concr. Res.* 54 (2013) 77–86, <https://doi.org/10.1016/j.cemconres.2013.08.005>.
- [59] T.R.S. Prasanna, A. Navrotsky, Energetics in the brownmilleriteperovskite pseudobinary  $\text{Ca}_2\text{Fe}_2\text{O}_5-\text{CaTiO}_3$ , *J. Mater. Res.* 9 (12) (1994) 3121–3124.
- [60] A. Gloter, J. Ingrin, D. Bouchet, K. Scrivener, C. Colliex, TEM evidence of perovskite-brownmillerite coexistence in the  $\text{Ca}(\text{Al}_x\text{Fe}_{1-x})\text{O}_{2.5}$  system with minor amounts of titanium and silicon, *Phys. Chem. Miner.* 27 (7) (2000) 504–513.
- [61] C. McCammon, A.I. Becerro, F. Langenhorst, R.J. Angel, S. Marion, F. Seifert, Short-range ordering of oxygen vacancies in  $\text{CaFe}_x\text{Ti}_{1-x}\text{O}_{3-x/2}$  perovskites ( $0 < x < 0.40$ ), *J. Phys. Condens. Matter.* 12 (2000) 2969–2984.
- [62] V.V. Sharygin E.V. Sokol Y.e. Vapnik Minerals of the pseudobinary perovskite-brownmillerite series from combustion metamorphic larnite rocks of the Hatrumim Formation (Israel) *Russ. Geol. Geophys.* 49 10 2008 2008 709 726.
- [63] P. Ptáček, T. Opravil, F. Šoukal, J. Havlica, R. Holesínský, Kinetics and mechanism of formation of gehlenite,  $\text{Al}_2\text{Si}$  spinel and anorthite from the mixture of kaolinite and calcite, *Solid State Sci.* 26 (2013) 53–58, <https://doi.org/10.1016/j.solidstatesciences.2013.09.014>.
- [64] R. Snelling, M. De Schepper, K. De Buysser, I. Van Driessche, N. De Belie, Clinkering Reactions During Firing of Recyclable Concrete, *J. Am. Ceram. Soc.* 95 (2012) 1741–1749, <https://doi.org/10.1111/j.1551-2916.2012.05168.x>.
- [65] M. Gallardo, J.M. Almanza, D.A. Cortés, J.C. Escobedo, J.I. Escalante-García, Synthesis and mechanical properties of a calcium sulfoaluminate cement made of industrial wastes, *Mater. Construcc.* 64 (315) (2014) e023, <https://doi.org/10.3989/mc.2014.04513>.
- [66] I. Jawed, J. Skalny, Alkalies in cement: A review I. Forms of Alkalies and their effect on clinker formation, *Cem. Concr. Res.* 7 (1997) 719–729, [https://doi.org/10.1016/0008-8846\(77\)90056-4](https://doi.org/10.1016/0008-8846(77)90056-4).
- [67] H.E. Exner, G. Petzow, A critical assessment of porosity coarsening during solid state sintering, *Adv. Sci. Technol.* 45 (2006) 539–548, <https://doi.org/10.4028/www.scientific.net/AST.45.539>.
- [68] R.K. Bordia, S.-J. Kang, E.A. Olevsky, Current understanding and future research directions at the onset of the next century of sintering science and technology, *J. Am. Ceram. Soc.* 100 (6) (2017) 2314–2352.
- [69] G.C. Lai, T. Nojiri, K. Nakano, Studies of the stability of  $\beta\text{-Ca}_2\text{SiO}_4$  doped by minor ions, *Cem. Concr. Res.* 22 (1992) 743–754.
- [70] K. Morsli, Á.G. de la Torre, S. Stöber, A.J.M. Cuberos, M. Zahir, M.A.G. Aranda, Quantitative phase analysis of laboratory-active belite clinkers by synchrotron powder diffraction, *J. Am. Ceram. Soc.* 90 (10) (2007) 3205–3212, <https://doi.org/10.1111/j.1551-2916.2007.01870.x>.
- [71] Z. Yanwei, Y. Nanru, A comparative study of the ferrite phase in high-iron cements with the pure  $\text{C}_2\text{AxF}_{1-x}$  by Mössbauer spectroscopy, *Cem. Concr. Res.* 21 (1) (1991) 31–37, [https://doi.org/10.1016/0008-8846\(91\)90028-G](https://doi.org/10.1016/0008-8846(91)90028-G).
- [72] K.S. Aleksandrov, B.V. Beznosikov, Hierarchy of perovskite-like crystals (review), *Fizika Tverdogo Tela.* 37 (1997) 785–808.
- [73] R. Bucchi, Feature on the role of minor compounds in cement clinker – part 1, *World Cem. Technol.* (1981) 210–231.
- [74] V. Morin, P. Termkhajornkit, B. Huet, G. Pham, Impact of quantity of anhydrite, water to binder ratio, fineness on kinetics and phase assemblage of belite-ye'elimite-ferrite cement, *Cem. Concr. Res.* 99 (2017) 8–17, <https://doi.org/10.1016/j.cemconres.2017.04.014>.
- [75] D. Shang, M. Wang, Z. Xia, S. Hu, F. Wang, Incorporation mechanism of titanium in Portland cement clinker and its effects on hydration properties, *Constr. Build. Mater.* 146 (2017) 344–349, <https://doi.org/10.1016/j.conbuildmat.2017.03.129>.
- [76] M.B. Marinho, F.P. Glasser, Polymorphism and phase changes in the ferrite phase of cements induced by titanium substitution, *Cem. Concr. Res.* 14 (3) (1984) 360–368.
- [77] M. Sato, E. Kojima, H. Uehara, M. Miyake, Si, Al solid solution in sodalite: synthesis  $^{29}\text{Si}$  NMR and X-ray structure, *Progress in Zeolite and Microporous Materials, Stud. Surf. Sci. Catal.* 105 (1997) 509–516.
- [78] T. Moteki, W. Chaikittisilp, Y. Sakamoto, A. Shimajima, T. Okubo, Role of Acidic Pretreatment of Layered Silicate RUB-15 in Its Topotactic Conversion into Pure Silica Sodalite, *Chem. Mater.* 23 (15) (2011) 3564–3570, <https://doi.org/10.1021/cm201480x>.
- [79] F. Winnefeld, L.H.J. Martin, C.J. Müller, B. Lothenbach, Using gypsum to control hydration kinetics of CSA cements, *Constr. Build. Mater.* 155 (2017) 154–163, <https://doi.org/10.1016/j.conbuildmat.2017.07.217>.
- [80] M. Zajac, J. Skocek, C. Stabler, F. Bullerjahn, F.M. Ben Haha, Hydration and performance evolution of belite-ye'elimite-ferrite cement, *Adv. Cem. Res.* 31 (2019) 124–137, <https://doi.org/10.1680/jadcr.18.00110>.
- [81] F. Winnefeld, B. Lothenbach, Hydration of calcium sulfoaluminate cements – experimental findings and thermodynamic modelling, *Cem. Concr. Res.* 40 (8) (2010) 1239–1247, <https://doi.org/10.1016/j.cemconres.2009.08.014>.
- [82] A. Schöler, B. Lothenbach, F. Winnefeld, M. Ben Haha, M. Zajac, H.M. Ludwig, Early hydration of SCM-blended Portland cements: A pore solution and isothermal calorimetry study, *Cem. Concr. Res.* 93 (2017) 71–82, <https://doi.org/10.1016/j.cemconres.2016.11.013>.
- [83] S. Kramer, L. Korat, M. Borštnar, A. Ipavec, L. Žibret, Pore evolution during sintering of the belite-sulfoaluminate cement clinker by X-ray computed microtomography, *Mater. Technol.* 54 (2020) 705–713, <https://doi.org/10.17222/mit.2020.031>.
- [84] M. Borštnar, N. Daneu, S. Dolenc, Phase development and hydration kinetics of belite-calcium sulfoaluminate cements at different curing temperatures, *Ceram. Int.* 46 (18) (2020) 29421–29428, <https://doi.org/10.1016/j.ceramint.2020.05.029>.
- [85] M. Borštnar, C.L. Lengauer, S. Dolenc, Quantitative in situ X-ray diffraction analysis of early hydration of belite-calcium sulfoaluminate cement at various defined temperatures, *Minerals-Basel* 11 (2021) 1–21, <https://doi.org/10.3390/min11030297>.
- [86] S. Dolenc, K. Šter, M. Borštnar, K. Nagode, A. Ipavec, L. Žibret, Effect of the cooling regime on the mineralogy and reactivity of belite-sulfoaluminate clinkers, *Minerals-Basel* 10 (2020) 1–16, <https://doi.org/10.3390/min10100910>.